New technique for electron-tunneling junction fabrication and its application to tantalum and niobium

V. Keith* and J. D. Leslie
Department of Physics, University of Waterloo, Waterloo, Ontario, Canada N2L 3G1
(Received 26 August 1977; revised manuscript received 7 March 1978)

A new technique for the fabrication of electron-tunneling junctions is presented. Ion etching is used to provide a hole in an insulating layer to define the junction area and to produce a clean surface of the underlying superconductor, as indicated by Auger electron spectroscopy, prior to the barrier formation and the evaporation of the counterelectrode. Knee structure in the current-voltage characteristics of $Ta-Ta_xO_y-Pb$ and $Nb-Nb_xO_y-Pb$ tunneling junctions above the voltage corresponding to the sum of the energy gaps is shown to be due to a proximity effect between a thin ion implanted normal layer and the underlying superconductor, and can be explained quantitatively using McMillan's theory of the proximity effect. Lowering the energy of the etching ions is shown to reduce the thickness of this normal layer and the associated proximity-induced structure in the tunneling characteristics, so that good values for Δ_{Ta} and Δ_{Nb} are obtained. It is proposed that the excess current observed below the voltage corresponding to the sum of the energy gaps is due to tunneling through normal regions of Nb or Ta in parallel with tunneling through the superconducting regions.

I. INTRODUCTION

The fabrication of an electron-tunneling junction requires a clean surface on the metal to be investigated, covered by a thin tunneling barrier of approximately 20 Å (usually the oxide of that metal) and a counterelectrode which is electrically isolated from the first metal except for a small area (usually less than 1 mm^2) where it contacts the tunneling barrier to make the metal-insulator-metal tunneling junction. In the classic work of Giaever[1] this was accomplished by evaporating an aluminum strip onto a microscope slide, allowing the clean surface of this freshly deposited aluminum strip to oxidize thermally in an oxygen atmosphere to a limiting thickness of approximately 20 Å, and then evaporating a cross strip of another metal to form the tunneling junction at the intersection of the two strips. Since that time, this basic approach to tunnel junction fabrication has been used for many different metals in many different tunneling investigations, particularly those associated with superconductive behavior. (For a recent review, see Solymar.[2])

However, not all metals can be fabricated into tunnel junctions by this evaporated-crossed-strips technique. Some metals are very reactive and getter active gases during the deposition process, so that the evaporated or sputtered film is not representative of bulk material. Certain materials may be difficult to evaporate, either because they evaporate only at very high temperature or because they are alloys and the constituents have very different vapor pressures. Also, there has been much interest in tunneling into single crystals, which are difficult to obtain in a controlled manner with an evaporated film. For all these reasons, there have been many investigations concerned with tunneling into bulk samples. However, in general, the techniques for obtaining a clean surface on the bulk sample, isolating the tunnel junction area, and forming the tunneling barriers have been specific to the material being studied. (See Table 23.1 in Solymar.[2]) Only the metal point contact[3] and the semiconductor point contact[4] have been proposed as general solutions to the problem of tunneling into bulk samples. While they give good results in certain cases, they still suffer from the problems of cleaning the tip and the surfaces of the bulk material to be investigated, prior to contact, and of nonideal tunneling characteristics resulting from nonuniformity of the tunneling barrier.

In this paper, we present a new approach to electron-tunneling junction fabrication which utilizes surface physics techniques such as ion etching and Auger electron spectroscopy. While our technique has been applied primarily to tunneling into bulk polycrystalline samples of tantalum and niobium to study their superconductivity, we feel that our technique is more general and could be applied to a whole range of other superconductors including alloys and single crystals. However, it must be emphasized that our technique is still in the development stage. As will be demonstrated later in this paper, ion etching produces a thin layer on the surface of the etched sample which is contaminated with implanted etching ions. On many superconductors with large coherence lengths, this ion implanted

layer would have negligible effects on the tunneling characteristics. However, on tantalum and niobium, with their short coherence lengths, this ion implanted layer produces a proximity sandwich which has major effects on the tunneling characteristics. We have used this side effect to study the proximity effect in tantalum and niobium. However, during the course of this investigation, we found that we could reduce substantially the thickness of this ion implanted layer, and hence its effects on the tunneling characteristics, by progressively reducing the energy of the ion etching beam. In this manner we have been able to almost eliminate structure in the tunneling characteristics of our tantalum junctions due to the proximity effect. We feel that a further reduction in the thickness of this ion implanted layer is possible through an even lower energy ion etching beam.

We chose tantalum and niobium as the first materials to use in our new technique for electron-tunneling junction fabrication for two reasons. First, these materials are difficult to tunnel into, and so they constitute a good test of the technique. Secondly, there is renewed interest in the tunneling into tantalum and particularly niobium as the result of recent measurements of Bostock *et al.*[5-8] and Robinson *et al.*[9,10] and so other tunneling results on these materials are of intrinsic interest.

Electron tunneling into transition metals such as tantalum and niobium has proven to be difficult because of the high chemical reactivity of the clean surfaces of these materials. Shen[11] points out that the electron-tunneling technique samples one coherence length beyond the insulating oxide at low energies and that this distance decreases to the electron mean free path at the higher energies associated with the phonons producing superconductivity. The coherence length is much shorter in transition metals than it is in sp-band materials such as lead. McMillan and Rowell[12] point out that this sampling distance is less than 500 Å for lead at energies greater than 9 meV. For transition metals, which have a smaller Fermi velocity, this sampling distance is approximately 100 Å. Shen[13] calculated this sampling distance for tantalum to be approximately 7.6 μm at 1 meV above the gap energy, approximately 120 Å at 11.4 meV (the transverse phonon energy) and 60 Å at 18 meV (the longitudinal phonon energy).

A contaminated surface layer of 50 to 100 Å on a transition metal thus may represent a substantial portion of the distance sampled in a tunneling experiment. This fact explains why it is difficult to tunnel into these materials and even obtain a good energy-gap value. The variation of the sampling distance with the energy of the electron tunneling explains why the phonon structure at high energy in the tunneling characteristics may be too weak even when at lower energy the tunneling characteristic is giving the correct value for the superconducting energy gap. So contaminated surfaces are most important in tunneling investigations of niobium and tantalum and other d- and f-band superconductors, in that they can influence the tunneling results and cause the observed properties to be nonrepresentative of the bulk material.

In Sec. I of this paper, we have presented an introduction to the problems of tunneling into transition metals. In Sec. II, we present details of our technique for junction fabrication on bulk materials. In Sec. III, we present our experimental results on tunneling into tantalum and niobium, including our proximity effect measurements, energy-gap measurements, and our conductance measurements, and a preliminary attempt to tunnel into La_3Al using our new technique. Finally in Sec. IV, we present the conclusions of our experimental results.

II. JUNCTION FABRICATION

The technique that we have developed for the fabrication of electron tunneling junctions involves ion etching[14] a hole through an insulating layer on the surface of the superconducting sample until Auger electron spectroscopy[15] indicates that a clean surface of the superconductor has been attained. Then thermal or plasma oxidation of the clean surface at the bottom of the hole produces the tunneling barrier, and finally a metal evaporation over the hole completes the tunnel junction. See Fig. 1 for a schematic representation of the resulting tunnel junction.

The superconducting substrate can take the form of a foil or a thin bulk slice provided that the surface is reasonably flat. Here we present the details of the technique used for junction fabrication

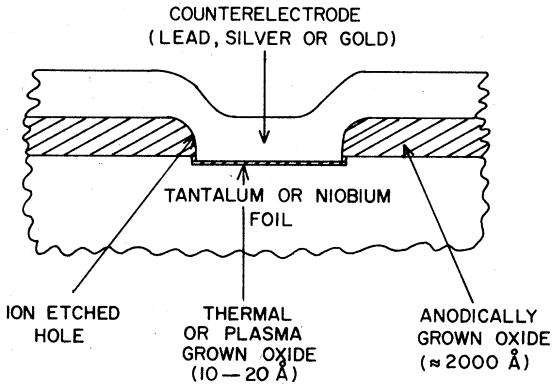

FIG. 1. Electron tunnel junction configuration.

on polycrystalline niobium and tantalum. Two types of superconducting samples have been used. The first type consisted of 0.005-in. polycrystalline foil cut to size $\frac{17}{32}$ in. by $\frac{3}{16}$ in., while the second type consisted of a $\frac{1}{16}$-in. thick disc of $\frac{1}{4}$-in. diameter, spot welded onto one of the standard-size foils. The foils were attached to the discs for clamping purposes and to allow electrical contacts to be made to both types of samples in the same manner in the sample holder used for measuring the tunneling characteristics. Spot welding was used because we wanted to try heating the discs close to their melting point in some of the experiments, but other methods of attachment are also possible. The discs were sliced on a wire saw or spark cutter from $\frac{1}{4}$-in. diameter polycrystalline rod. Both cutting techniques left a jitter on the face of the samples, which were subsequently polished mechanically to a quarter micron finish.

The samples were washed in acetone and then the contaminated and strained surface layers were removed with a chemical etch consisting of 50 ml of concentrated sulphuric acid, 20 ml of concentrated nitric acid, and 20 ml of concentrated hydrofluoric acid. A 20-sec etch was sufficient to remove the contaminated and deformed surface layers, and then the samples were washed with distilled water to remove all traces of the etchant.

The insulating layer on the clean surfaces of these samples was formed by anodic oxidation.[16] The electrolytic cell consisted of a platinum cathode, 0.2N sulphuric acid electrolyte, and the sample acting as the anode. The anodic oxide was grown at constant anode current until a desired anode voltage had been reached. The thickness of the anodic oxide grown is proportional to the anode voltage, and we used the results of Ord *et al.*[17] to calibrate the thickness of our oxide layers. For tantalum, the oxide thickness grown per volt is 17.25 Å and for niobium it is 25 Å. Typically a 2000 Å thick oxide was grown on the surface of the samples as the insulating layer. The samples were washed with distilled water to remove all traces of the electrolyte. A final wash with acetone removed the water and accelerated the drying process.

The oxidized samples were then carefully mounted on a carousel specimen manipulator (model 10-502) of a Physical Electronics Industries Auger electron spectrometer. The specimen manipulator has six degrees of mechanical freedom: X, Y, and Z translations, tilt about two orthogonal axes, and 360° rotation. The six degrees of freedom allow precision positioning of the samples in the vacuum chamber of the Auger system. The specimen manipulator has four high-current feedthroughs connected to a specially designed current commutator, which allows the heating of an individual sample by passing a current through it, enabling degassing of the sample in an ultrahigh vacuum. A specially designed sample stage on the specimen manipulator can accommodate ten samples, but only five of them can be fabricated into complete tunnel junctions. Each of the five tunnel junction positions on the sample stage is fitted with two masks. The first has a hole 0.5 mm in diameter and is used for ion etching a hole through the insulating layer. The mask is hinged and can be flipped out of the way allowing a second mask to be flipped into position over the sample. This second mask has a slit 0.25 in. by 0.06 in. which defines the area for the final metal evaporation. The mask manipulation was accomplished with a mask flipping lever which could be operated from outside the vacuum chamber by means of a rotary ultrahigh-vacuum (UHV) seal.

With the specimen manipulator in position and all flanges tightened, the vacuum chamber of the Auger system was pumped down to less than 5×10^{-3} Torr pressure by means of two liquid nitrogen cooled sorption pumps. The sorption pumps were then isolated from the Auger system by closing a UHV valve in the pumping line. The poppet valve between the ion pump chamber and the main vacuum space was then opened slowly, while keeping the pressure below 2×10^{-5} Torr in the ion pump chamber. Once the poppet valve was completely open, the pressure in the vacuum system reached the 10^{-8} Torr range within an hour. From time to time a titanium sublimation pump was used to deposit a fresh layer of titanium to trap the active gases and speed the pump down. With overnight pumping and a bakeout to less than 200 °C, a pressure in the 10^{-10} Torr range was easily achieved.

At this point the samples were ready for ion etching the tunnel junction area holes through the insulating layer. A fresh layer of titanium was deposited on the trapping surface of the titanium sublimation pump, and then the ion pump was turned off. An inert gas, i.e., argon, krypton, or xenon, was admitted to the vacuum system through a Varian leak valve until the pressure reached 5×10^{-5} Torr. The titanium layer held the pressure inside the vacuum chamber at this value during the ion etching by selectively pumping any active gases released. The sample to be etched was aligned so that the electron beam from the electron gun in the cylindrical mirror analyzer passed through the 0.5-mm-diam hole in the ion etch mask and was focused as a spot of approximately 0.1-mm-diameter on the surface of the sample. The secondary electrons coming from

this 0.1-mm-diam spot were collected and analyzed by the cylindrical mirror analyzer and associated electronics to produce an Auger spectrum of the surface of the sample in the center of the 0.5-mm-diam junction area defined by the hole in the ion etching mask. The ion etching beam is much broader than the hole in the ion etching mask, and so the sample surface is etched uniformly across the 0.5-mm-diam circle that is exposed to the ion beam.

It is possible to ion etch and take an Auger spectrum at the same time. Since Auger spectroscopy yields information about the atomic elements within 10 to 20 Å of the surface of the sample, when combined with ion etching, it allows one to obtain a depth profile of the atomic constituents of a sample. The Auger spectra can be analyzed to yield the atomic concentrations of each of the elements present at the exact location of the tunneling barrier. This gave us great control over the conditions during the fabrication of a tunnel junction. We knew exactly when the insulating layer had been etched through, what impurities were present, and finally when the uncontaminated material had been exposed at the bottom of the tunnel junction area hole by the ion etch.

One limitation of our fabrication technique is the fact that the etching ions also implant[18] a certain distance R_p into the surface. We made use of this side effect to study the proximity effect resulting from this ion implanted normal layer on top of the bulk superconductor, and our results are described in Sec. III. Since the distance R_p is proportional to E, the energy of the ions, successive reduction of the ion beam energy resulted in the decrease of the depth to which the ions were being implanted. After the "pure" material had been exposed by the 2-keV ion beam etch, the voltage on the ion gun was reduced to 500 V in steps of 500 V. In the case of argon ions, the depth of implantation in tantalum reduced from 10.8 Å at 2 keV to 2.7 Å at 500 eV. To obtain tunnel junctions which showed a minimum of a proximity effect, this beam voltage reduction process was essential.

Once the hole had been etched through the insulating layer and the Auger spectra indicated that a suitably clean surface of the superconductor had been reached, the sample was ready for the formation of the tunneling barrier. A final Auger spectrum was taken so that the atomic concentrations of the impurities present on the freshly exposed surface of the superconductor could be determined later. After turning off the electron gun in the cylindrical mirror analyzer and allowing it to cool for a couple of minutes, the ion pump was used to pump out the inert gas and then the ion pump was again isolated from the vacuum system, and oxygen was admitted through a Varian leak valve to a pressure of 50 μm. Both niobium and tantalum oxidize very readily in an oxygen atmosphere at room temperature, and it was easy to grow an oxide layer of approximately 20 Å on the exposed surface of the superconductor to form the tunneling barrier. We also successfully formed tunneling barriers using plasma oxidation. A voltage of -900 V was applied to a cathode made of tantalum or niobium via a high-voltage feedthrough, and the sample was made slightly positive with respect to ground. The plasma oxidation was carried out in the Auger system at 50 μm of oxygen pressure. The plasma was kept glowing greenish-white for approximately 2 min to give a sufficiently thick oxide barrier for tunneling.

The final stage of the junction fabrication was to evaporate the counterelectrode. After the 50 μm of oxygen pressure had been reduced to less than 5 μm by use of the sorption pumps, the ion pump was used to reduce the pressure to the 10^{-9} Torr range. Since the system had not been exposed to water vapor, the pump down was accomplished in a few minutes. The Auger system contained an evaporator with specially designed evaporation sources that allowed evaporation in the forward horizontal direction only. The evaporation sources were outgassed prior to the ion etch process in order not to contaminate the samples during the final evaporation of the counterelectrode. Note that it is more important to avoid contamination on the niobium or tantalum side of the junction barrier than it is on the evaporated counterelectrode side, since the sampling distance is much shorter in the transition metals and since they are generally more reactive. The sources were heated slowly to maintain a pressure below 5×10^{-7} Torr at all times during the evaporation. When the quartz-crystal thickness monitor indicated that the evaporation had begun, the sample was rotated into position and approximately 3 000 Å of lead, silver, or gold were evaporated to form the counterelectrode. The quartz-crystal thickness monitor was calibrated by means of an optical interferometer.

Once all the tunneling samples had their counterelectrodes evaporated, the junction preparation was complete and the samples could be removed from the Auger system without danger of contamination of the junction area except for that due to internal diffusion processes. The prepared junctions were then mounted one at a time on a sample holder for measurement of the I vs V, dV/dI vs V, and d^2V/dI^2 vs V tunneling characteristics at helium temperature.

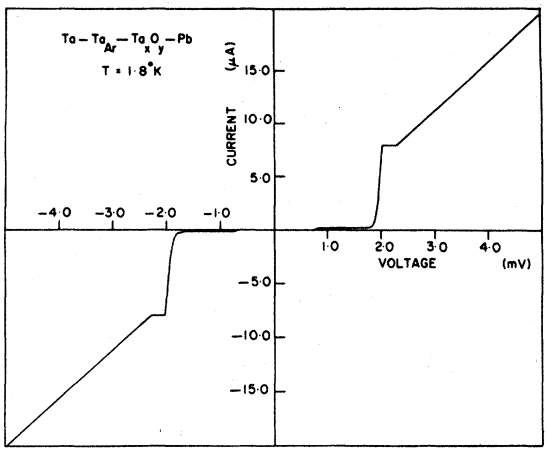

FIG. 2. Current-voltage characteristic of a Ta-Ta$_{Ar}$ – Ta$_x$O$_y$ – Pb tunnel junction fabricated using a 2-keV argon-ion etch.

III. EXPERIMENTAL RESULTS AND ANALYSIS

A. Tantalum

Figure 2 shows a typical current-voltage characteristic of a tunnel junction fabricated on a polycrystalline Ta foil using the procedure outlined in Sec. II. The ion etching was done using a 2-keV beam of argon ions. We designate this type of junction as a Ta-Ta$_{Ar}$-Ta$_x$O$_y$-Pb tunnel junction, because the substrate is Ta with an argon-doped surface layer, the tunneling barrier is tantalum oxide, and the counterelectrode is Pb. The effect of the argon-doped surface layer will be discussed later in this section.

Figure 3 shows a typical Auger electron spectrum of the surface of the Ta at the center of hole defining the tunneling area after the completion of the 2-keV argon-ion etch, but before the oxidation and the evaporation of the counterelectrode to form the type of tunnel junction whose I-V characteristic is given in Fig. 2. Such an Auger electron spectrum can be analyzed to determine the atomic concentration C_x of the elements x present on the surface and within a 20-Å layer below the surface, using the standard spectra and the following approximate formula from the Handbook of Auger-Electron Spectroscopy[19]:

$$C_x = \frac{I_x}{S_{x,\mathrm{Ag}}} \Big/ \sum_{\alpha} \frac{I_\alpha}{S_{\alpha,\mathrm{Ag}}}, \tag{1}$$

where the sum in Eq. (1) is over one peak in the Auger electron spectrum for each element present on the surface. I_x is the peak-to-peak height of that one of the peaks, associated with element x

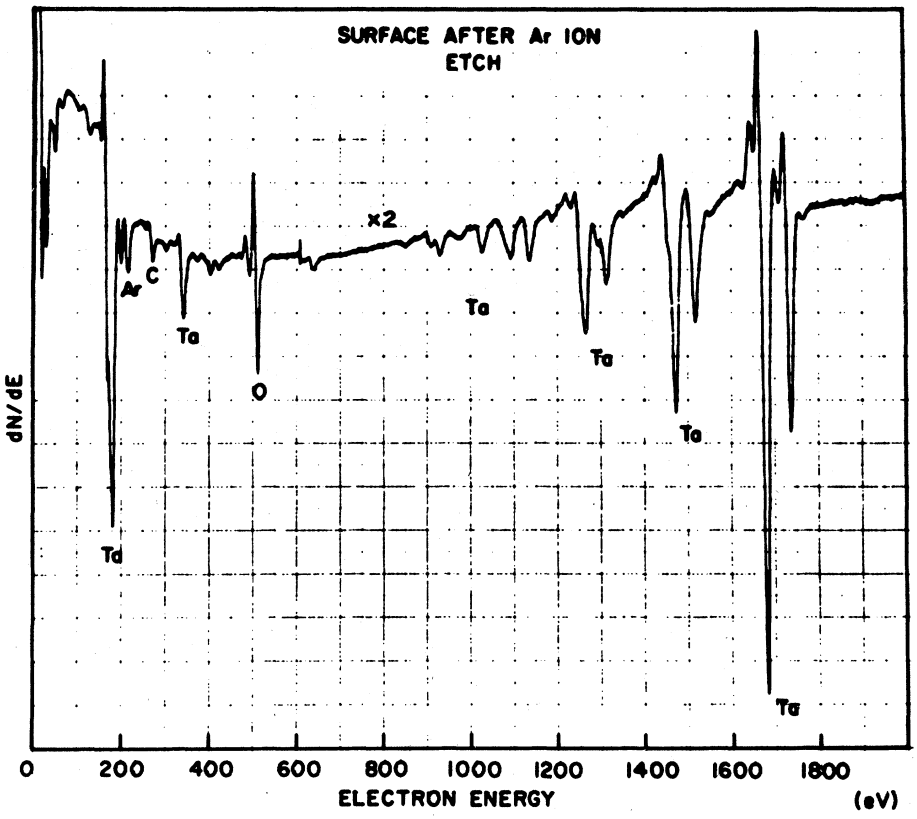

FIG. 3. Auger spectrum of the surface of a Ta foil at the center of the junction area after the argon-ion etch.

TABLE I. Atomic concentrations of the various elements present on the surface of a Ta foil in the center of the junction area after the argon-ion etch.

	Final			
Element	C	O	Ta	Ar
I_α	60	260	380	24
$\frac{I_\alpha}{S_{\alpha,\mathrm{Ag}}}$	542.50	509.20	6418.92	830.45
C_α	6.5%	6.1%	77.3%	10.1%
	Without argon			
C_α	7.3%	6.8%	85.9%	

in the experimentally determined dN/dE vs E Auger spectrum, which is chosen to characterize the element x. $S_{x,\mathrm{Ag}}$ is the relative sensitivity of the Auger peak of element x compared to that of Ag and is found from

$$S_{x,\mathrm{Ag}} = I_x^H/(K_x I_{\mathrm{Ag}}^H)\,, \tag{2}$$

where I_x^H and I_{Ag}^H are the corresponding peak-to-peak heights of the standard spectra in the Handbook of Auger Electron Spectroscopy for element x and Ag, respectively. K_x is the scale factor associated with the standard spectrum for element x.

The results of analyzing Fig. 3 in this manner are presented in Table I. The exact concentration of argon in the argon-doped surface layer cannot be determined for the following reason. The standard spectrum for Ar is that for an unknown concentration of Ar embedded into Si. In the quantitative analysis given in Table I, we have treated this spectrum as corresponding to 100-at.% Ar, and on this basis we arrive at a concentration of 10.1-at.% Ar. This assumption is obviously not true, and the percentage of Ar determined in this way is just an upper limit. We have also shown in Table I an analysis for the concentration of C, O, and Ta omitting the peak associated with Ar from the analysis.

The current-voltage characteristics, shown in Fig. 2, of tunnel junctions fabricated on surfaces with the amount of impurities indicated in Table I have very little excess current below the voltage corresponding to the sum of the energy gaps. We use the voltage corresponding to the midpoint of the current rise as the definition of the sum of the energy gaps. However, the resulting value of $\Delta_{\mathrm{Pb}}+\Delta_{\mathrm{Ta}}$ is only 1.95 meV which yields a value of 0.6 meV for Δ_{Ta}, since we measure Δ_{Pb} to be 1.35 meV. As shown later in Table II, a value of 0.70 to 0.72 meV is the more accepted value for Δ_{Ta}.

The I-V characteristic of Fig. 2 also shows some structure just above the voltage corresponding to the sum of the energy gaps. The ion etching process used in the fabrication of our tunnel junctions leaves etching ions as impurities in the surface layer of the sample being cleaned. We would like to show that the "knee" structure that we observe in our samples is the result of a proximity effect between this ion implanted layer and the underlying superconductor and that it can be explained in terms of the McMillan tunneling model[20] (MTM) of the proximity effect. The knee structure shown in Fig. 2 becomes smaller and less pronounced as the temperature is increased, and eventually disappears.

Similar knee structure in I-V characteristics has been observed in a number of earlier tunneling investigations.[11,21,22] Shen[11] observed knee structure in the earliest tunneling experiments with tantalum and niobium. He attributed it to a thin layer of normal metal on the surface of the superconductor caused by insufficient outgassing of the carbon in his foil samples. He suggested that the proximity effect between this normal metal layer and the underlying superconductor could account for the knee, but no fit to MTM was presented. Wyatt *et al.*[21] observed knee structure in Pb–Zn-oxide–Pb junctions even when the Zn layer was as thin as 5 Å. They showed that MTM could qualitatively explain their results. Frommer *et al.*[22] observed knee structure in tunneling experiments with niobium single crystals. They suggested that carbon contamination was a remote possibility due to the method of preparing their samples, and they proposed an alternative mechanism for the knee structure in terms of impurity tunneling caused by excess adsorbed oxygen in the oxide insulating barrier.

MTM[20] assumes that the normal (N) and superconducting (S) layers in the proximity sandwich are both thin, compared to a coherence length, and are separated by a thin insulating potential

TABLE II. Listing of the observed energy-gap values for tantalum.

Reference	$2\Delta_{\mathrm{Ta}}$(meV)
Townsend and Sutton (Ref. 31)	1.40 ± 0.05
Dietrich (Ref. 32)	1.42
Giaever (Ref. 33)	1.35 ± 0.05
Wyatt (Ref. 34)	1.40
Neugebauer and Ekvall (Ref. 35)	1.30 ± 0.05
Shen (Refs. 11, 13)	1.44
Keith and Leslie (This work)	1.40 ± 0.05

barrier. Coupling between the S and N layers is treated as a tunneling process involving the transmission of electrons through the barrier, and results in a decrease (increase) in the spatially constant order parameter in the S (N) layer. The important lifetime broadening parameters in MTM are

$$\Gamma_N = \hbar/\tau_N = \hbar v_F \sigma / 2Bd_N , \tag{3}$$

$$\Gamma_S = \hbar/\tau_S = \Gamma_N d_N N_N(0)/d_S N_S(0) , \tag{4}$$

where τ_N and τ_S are the lifetimes of an electron in the N and S layer, respectively. The thickness and the density of states in the S (N) layer are denoted by d_S (d_N) and $N_S(0)$ [$N_N(0)$], respectively. In Eq. (3), $2Bd_N$ is the average electron path length in the normal layer between collisions with the barrier; thus B, which McMillan estimates to be approximately unity for a clean layer, is a function of the ratio of the mean free path to the thickness d_N of the normal layer. The Fermi velocity and the barrier transmission probability are denoted by v_F and σ, respectively.

The energy-dependent and complex self-energies $\Delta_N(E)$ and $\Delta_S(E)$ are found by solving MTM Eqs. (16) numerically on a digital computer using an iterative procedure, given values for the lifetime broadening parameters Γ_N and Γ_S and the fixed BCS potentials $\Delta_N^{\rm ph}$ and $\Delta_S^{\rm ph}$. MTM Eq. (11) specifies the self-consistency condition on the BCS potentials. The self-energies $\Delta_{S,N}(E)$ are observable in their effect of the tunneling-electron density of states in the $S(N)$ layer, i.e., $N_{S,N}(E)$ which involves $\Delta_{S,N}(E)$ in the following manner:

$$N_{S,N}(E) = \mathrm{Re}\{E/[E^2 - \Delta_{S,N}^2(E)]^{1/2}\} . \tag{5}$$

The applicability of MTM has been studied in a number of investigations[23-26] by electron tunneling into the N or S sides of proximity sandwiches for various thicknesses of the N and S layers. The usual experimental measurement is that of the differential conductance of the tunnel junction which is related to the tunneling electron density of states $N_{S,N}(E)$. Early experiments[23,24] showed reasonable agreement with the general features of MTM. Vrba and Woods[25] showed that if the MTM requirement of weak coupling between the N and S layers was obtained by allowing slight oxidation to occur at the interface, then satisfactory quantitative agreement with MTM resulted. In most of their experiments, d_N was of the order of 100 Å and d_S was of the order of 1000 Å. They showed that in the fitting to MTM the properties of the proximity sandwich are strongly dependent on the value of Γ_N, but only weakly dependent on the value of Γ_S. A similar observation was made by Wyatt *et al.*[21] in their fitting of MTM to the knee structure they observed. Toplicar and Finnemore,[26] in the process of studying the effect on the phonon spectrum of Pb when it was in a proximity sandwich with Cd, examined the applicability of MTM in the limit that d_S is of the same order as d_N. They found reasonable agreement between their experimental tunneling conductances and the predictions of MTM.

The ion etching process used in the fabrication of our tunnel junctions leaves etching ions as impurities in the surface layer of the sample being cleaned. The depth R_p to which these ions are being implanted can be calculated from the following equations[18]:

$$R(\text{Å}) = \frac{60E(\text{keV})M_2}{g} \frac{(M_1+M_2)(Z_1^{2/3}+Z_2^{2/3})^{1/2}}{Z_2 \quad M_1 \quad Z_1} , \tag{6}$$

and

$$R/R_p = 1 + M_2/3M_1 , \tag{7}$$

where R is the total distance travelled by the ion before coming to rest, whereas R_p is the projected distance, i.e., the perpendicular distance below the surface of the sample that the ion reaches after travelling a total distance R. E is the energy of the bombarding ion and g is the density of the target in g/cm^3. Z and M are the atomic number and mass, and the subscripts 1 and 2 refer to the ion and target atoms, respectively. A calculation based on Eqs. (6) and (7) indicated that 2-keV argon ions would penetrate a tantalum target to a depth of approximately 10 Å. Auger electron spectroscopy of the argon-ion etched surface had already shown the presence of argon ions on the surface of the cleaned Ta in agreement with this calculation.

In order to do a self-consistent fit to MTM, one needs information about bulk properties of the S and N layers, e.g., the value of the pairing interaction λ and the characteristic phonon energy ω_c for each layer.[20,25] If $\Delta_S^{\rm ph}$ is to be used as the one parameter fitted to experiment, one needs the sample transition temperature T_c, the bulk superconductor transition temperature T_{cs}, and the density of states $N(0)$, in addition to the thicknesses d_N and d_S.[20,26] In our case, we do not have information about the bulk properties of the thin (10 Å) argon-doped layer and the shift in T_c caused by such a thin layer on a superconducting foil 0.005 in. thick cannot be detected. Consequently, in our fit to MTM we have had to make certain assumptions. We have taken d_N equal to R_p and we have assumed $\Delta_N^{\rm ph}$ to be 0.0 meV in all fits, which corresponds to taking λ_N equal to zero. MTM assumes that d_N and d_S are both small, compared to a coherence length, whereas our superconducting foils are many coherence lengths

thick. As shown in Eq. (4), the value of d_S influences the value of the MTM lifetime broadening parameter Γ_S. It has been shown[21,25] that when d_N is a small fraction of d_S, the fit to MTM is rather insensitive to the value of Γ_S. Thus, we have taken Γ_S as an adjustable parameter which we start out at a value corresponding to a d_S = 2000 Å and then adjust it to get a better fit with the experimental results. Because of the small value of Γ_S/Γ_N used in our fits to MTM, Δ_S^{ph} is found to be equal to Δ_S^{bulk}.[25]

The applicability of MTM to describe the tunneling electron density of states $N_{S,N}(E)$ in proximity sandwiches has already been established.[23-26] We are interested in demonstrating that the knee structure that we observe in our I-V characteristics is due to a proximity effect which can be explained in terms of MTM. The tunneling current $I(V)$ is given by

$$I(V) = K \int_{-\infty}^{\infty} N_l(E - eV) N_r(E) [f(E - eV) - f(E)] dE , \tag{8}$$

where $N_l(E - eV)$ and $N_r(E)$ are the tunneling electron density of states for the metals on the left-hand side (l) and the right-hand side (r) of the tunneling barrier, respectively, $f(E)$ is the Fermi distribution function, K is a constant depending on the area and thickness of the tunneling barrier, E is the energy, and V is the applied voltage. In our case, if the proximity sandwich is considered to be on the right-hand side of the barrier, since we would be tunneling into the N layer of the proximity sandwich, $N_r(E)$ in Eq. (8) would become $N_N(E)$ from Eq. (5).

The first step in fitting the proximity induced structure in the I-V characteristics of our Ta-Ta_{Ar}-Ta_xO_y-Pb tunnel junctions was to obtain an estimate of the value of Γ_N. The Fermi velocity v_F for tantalum is approximately 0.24×10^8 cm/sec, and inserting this into Eq. (3), along with $B = 1$ and the value of $\hbar$, we obtain

$$\Gamma_N = 790\sigma/d_N . \tag{9}$$

Adkins and Kington[23] estimate $\sigma = 0.1$ for copper and silver on the surface of lead films. From Eqs. (6) and (7), we have estimated the thickness of our argon-doped normal layer to be 10 Å. Substituting these values for σ and d_N into Eq. (9), we find $\Gamma_N = 8$ meV. Using this value of Γ_N, d_N = 10 Å and d_S = 2 000 Å, and assuming that $N_N(0) = N_S(0)$, we find that Eq. (4) gives $\Gamma_S = 0.04$ meV.

Using these estimates of Γ_N and Γ_S as a guide, we have solved numerically MTM Eqs. (16) for $\Delta_S(E)$ and $\Delta_N(E)$, using $\Delta_N^{ph} = 0.0$ meV and Δ_S^{ph} = 0.7 meV and several values of Γ_N and Γ_S. The

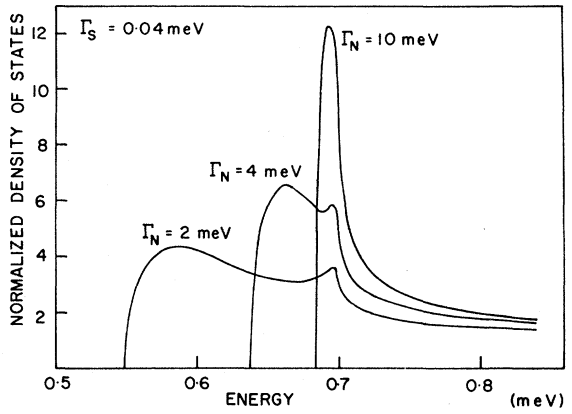

FIG. 4. Densities of states on the N side of a proximity sandwich, according to McMillan's theory of the proximity effect, used to calculate the tunneling curves of Fig. 5.

computed $\Delta_S(E)$ and $\Delta_N(E)$ were then used to calculate the tunneling electron density states $N_N(E)$ from Eq. (5), which was then substituted into Eq. (8) to generate the I-V characteristics of our Ta-Ta_{Ar}-Ta_xO_y-Pb tunnel junctions. The counter-electrode in this calculation was assumed to be a superconductor with a complex energy gap such that $\Delta^2 = 1.36^2 + 0.05\, i\,\text{meV}^2$ in order to give a smeared BCS density of states and the numerical values were chosen to be appropriate for Pb.

Figure 4 shows the tunneling electron density of states $N_N(E)$, calculated from Eq. (5), for tunneling into the N side of a proximity sandwich for several values of Γ_N. Figure 5 shows the corresponding current-voltage characteristics calculated from Eq. (8) for a Ta-Ta_{Ar}-Ta_xO_y-Pb tunnel junction. Figure 5 shows that as Γ_N is decreased, i.e., as d_N is increased, the proximity induced knee becomes more and more pronounced, and the voltage corresponding to the sum of the energy gaps, $\Delta_{Ta} + \Delta_{Pb}$, becomes smaller.

Figures 4 and 5 are just intended to show the general behavior of $N_N(E)$ and the I-V characteristic as a function of Γ_N. To make a final fit to our experimental I-V characteristic, we repeated the calculations leading to Fig. 5 for a range of Γ_N values while also varying Γ_S. Figure 6 shows the best fit to our experimental I-V curve for a Ta-Ta_{Ar}-Ta_xO_y-Pb tunnel junction achieved by using a value of 3.0 meV for Γ_N and 0.01 meV for Γ_S in the calculated I-V characteristics. Figure 6 shows that these calculations using MTM can reproduce both the observed voltage corresponding to the sum of the energy gaps and the magnitude and shape of the proximity induced knee in the I-V characteristics of our Ta-Ta_{Ar}-Ta_xO_y-Pb tunnel junctions. In fact, the quantitative agreement be-

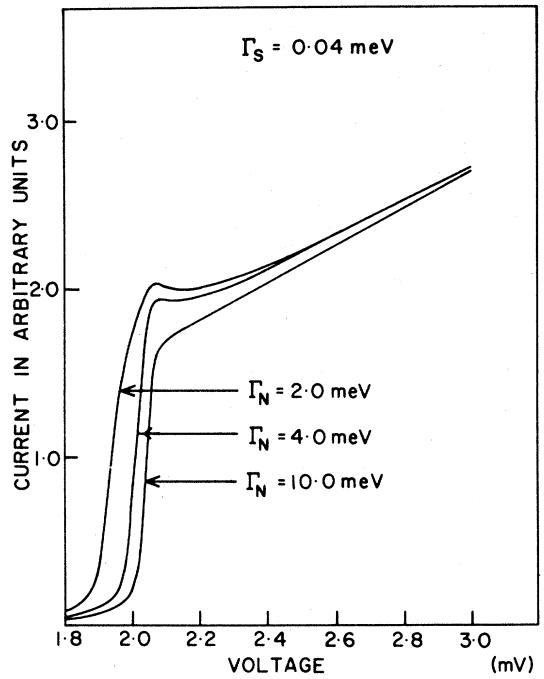

FIG. 5. Portion of the current-voltage characteristics predicted by McMillan's theory of the proximity effect for tunneling into the argon contaminated Ta side of a Ta_{Ar}-Ta proximity sandwich (with the parameters shown) from a Pb counterelectrode with a smeared energy gap and at a temperature of 1.5 °K.

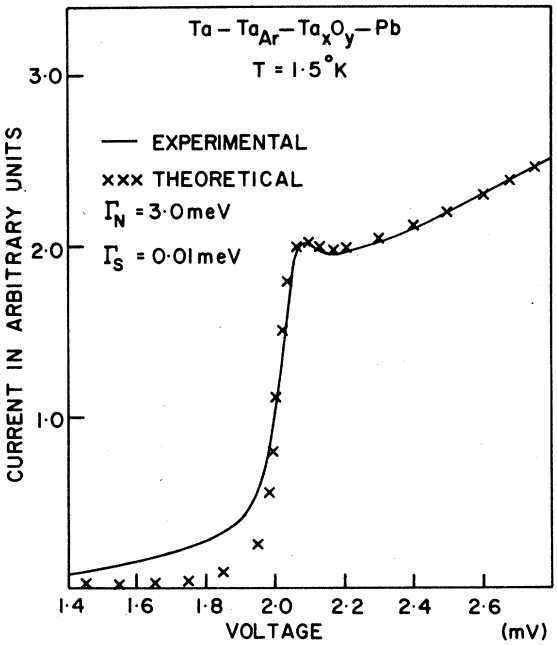

FIG. 6. Portion of the calculated current-voltage characteristic (×××) with Δ_S^{ph} = 0.70 meV, Δ_N^{ph} = 0.0 meV; Γ_S = 0.01 meV, and Γ_N = 3.0 meV compared with the experimental curve (solid line) for a Ta-Ta_{Ar}-Ta_x0_y-Pb tunnel junction at 1.5 °K.

tween the experimental and the calculated *I-V* characteristics for *V* greater than 2 mV in Fig. 6 is quite good, and this suggests that MTM describes the experimental situation quite well. However, the excess current for *V* less than 2 mV in Fig. 6 cannot be explained on the basis of MTM, nor can it be explained by increasing the imaginary part of the lead energy gap. If we ignore the poor fit in Fig. 6 for *V* less than 2 mV, which corresponds to the region $eV < \Delta_{Ta} + \Delta_{Pb}$, then we can establish a value for σ since we know from the theory of ion implantation that 2-keV argon ions are implanted to a depth of 10 Å in tantalum. From Eqs. (3) and (9)

$$\Gamma_N = \frac{\hbar v_F \sigma}{2Bd_N} = \frac{790\sigma}{d_N} = 3.0 \text{ meV} \tag{10}$$

therefore,

$$\sigma = \frac{3d_N}{790} = 0.04 (\text{for } d_N = 10 \text{ Å}) \tag{11}$$

which is smaller than the value of 0.1 for σ estimated by Adkins and Kington[23] for Cu and Ag on Pb. We leave further discussion of the value of σ until after the niobium tunneling results have been presented.

The origin of the excess current below the voltage corresponding to the sum of the energy gaps is possibly tunneling through regions which were left contaminated by impurities other than the implanted argon ions. One possible source of this contamination would be diffusion of impurities from the bulk of the sample to the surface along the grain boundaries.

If there are regions of tantalum which are normal, then we have an additional contribution to the current. We can divide the junction into two junctions in parallel, i.e., *a* Ta_S-Ta_{Ar}-Ta_xO_y-Pb junction in parallel with *a* Ta_N-Ta_xO_y-Pb junction, where Ta_S and Ta_N represent the superconducting and normal tantalum, respectively. Since the junctions are in parallel, we can add the currents at each voltage point. The contribution to the total current due to the normal region is

$$I_N = K' \int_0^\infty N_T(E)[f(E - eV) - f(E + eV)]dE, \tag{12}$$

where K' is a constant and the other symbols have their usual meanings as defined in Eq. (8).

The interpretation of *I-V* and $dI/dV - V$ characteristics in terms of models involving tunneling junctions in parallel has been employed previously in the literature.[27-29] Rowell and Schmidt[27] have suggested that one interpretation of the multiple gaps that they observe in tunneling into getter sputtered Nb_3Ge films is the presence of two phases within the surface of the film. Milkove

et al.[28,29] have shown that a model consisting of a series resistance in one leg of a parallel circuit containing two identical tunneling junctions can generate structure in the I-V and $dI/dV - V$ characteristics of the combination which is similar to that which has been attributed to anisotropy and multiple energy gaps.

We generated an I-V curve with this normal tunneling term included in the numerical calculation for a Ta-Ta_{Ar}-Ta_xO_y-Pb tunnel junction in which one tenth of the current contribution was from the normal regions of tantalum, i.e., $K/K' = 10$. The results showed that the excess current below the voltage corresponding to the sum of the energy gaps was due to normal regions of tantalum. The sharp onset of the excess current at approximately the energy gap of lead which is observed experimentally was reproduced in the calculated I-V characteristic as shown in Fig. 7, where we compare the I-V characteristics calculated for tunnel junctions with and without any normal regions of tantalum. This two junctions in parallel model is an oversimplification of the actual situation in that there is probably a range of material going from superconducting to normal and this would result in additional current contributions smearing out the excess current region below $eV = \Delta_{Ta} + \Delta_{Pb}$. Note that this normal tunneling contribution does not affect the value of the energy gaps or the phonon structure, except to make the latter a smaller fraction of the junction conductance, as derived from the tunneling characteristics of the junction.

Figure 8 shows the experimental I-V characteristics of three different Ta-Ta_xO_y-Pb tunnel junctions at 1.2 °K. Each one shows an onset of excess current at about 1.0 mV, but the amount of excess current is different in each case. One possible source of normal regions would be carbon[11] diffusing out from the interior of the sample along grain boundaries. However, we have not been able to prove this. For example, junction 3 was found to have a lower concentration of carbon at the center of the junction than junction 2, and yet the amount of excess current is greater for junction 3 than it is for junction 2. However, we cannot rule out carbon as the source of the normal regions on the basis of this evidence, since we did not check the carbon concentration at several spots on the junction area and we also did not control the time that the junction was exposed to possible contamination from the vacuum system prior to oxidizing and completing the tunnel junction.

We now return to the junction shown in Fig. 6 to try to fit the excess current below the voltage corresponding to the sum of the energy gaps. Figure 9 shows a much improved fit below eV

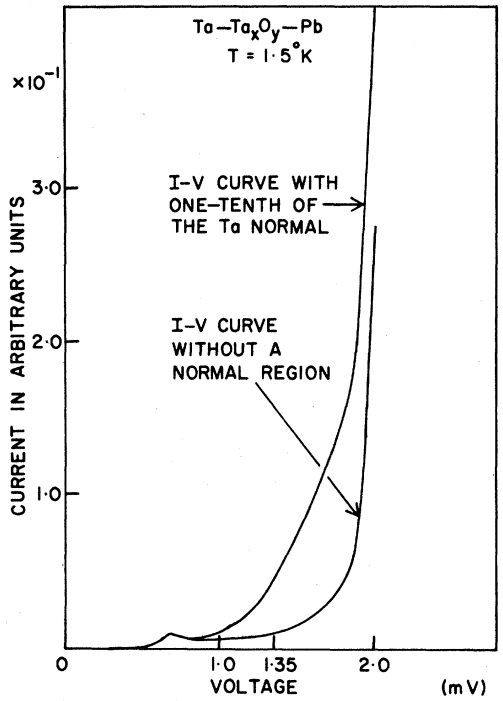

FIG. 7. Calculated current-voltage characteristic for a Ta-Ta_xO_y-Pb tunnel junction with one tenth of the current coming from normal Ta in the junction area compared with that for a Ta-Ta_xO_y-Pb tunnel junction without a normal Ta region.

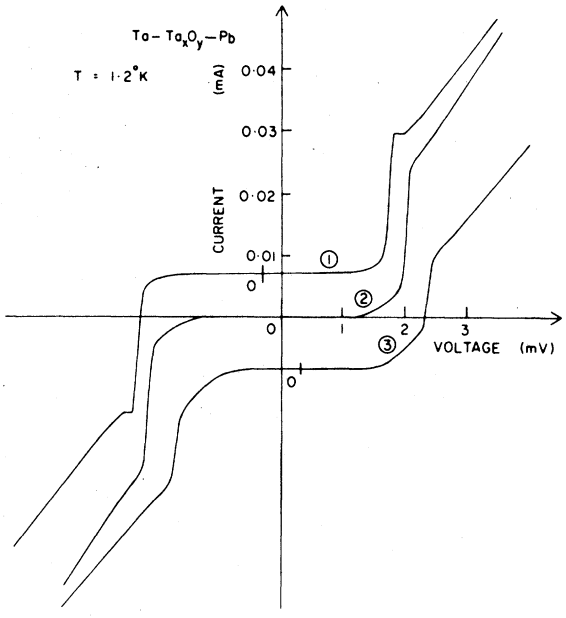

FIG. 8. Experimental current-voltage characteristics for Ta-Ta_xO_y-Pb tunnel junctions at $T = 1.2$ °K showing different amounts of excess current below $eV = \Delta_{Ta} + \Delta_{Pb}$.

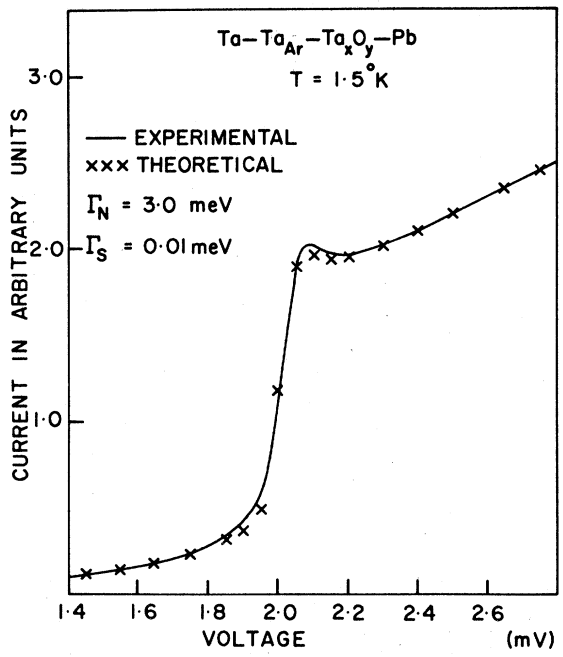

FIG. 9. Portion of the calculated current-voltage characteristic for a Ta-Ta$_{Ar}$-Ta$_x$O$_y$-Pb tunnel junction at $T = 1.5$ °K with 25% of the tunneling current coming from normal areas of the junction.

$= \Delta_{Ta} + \Delta_{Pb}$ at the expense of a small loss of agreement above $eV = \Delta_{Ta} + \Delta_{Pb}$. Further adjustment of the parameters Γ_S and Γ_N, to yield a sharper knee above $eV = \Delta_{Ta} + \Delta_{Pb}$, results in a poorer overall agreement since the energy-gap region begins to shift to too low an energy. The theoretical curve generated to fit the experimental data indicates that 25% of the current in the junction is coming from normal areas of the junction. However, this does not necessarily mean that 25% of the tantalum surface in this junction is behaving as normal metal, e.g., if the tunneling barrier were much thinner over these normal regions, then the actual area of normal regions needed could be much less. It is not certain, as we have stated earlier, whether it is the carbon impurity which is causing the tantalum to go normal. Another possibility is the generation of normal-state material by magnetic flux trapping often seen in type-II superconductors, as suggested by Testardi.[30] An argument against the latter possibility is that we should be able to trap different amounts of magnetic flux in the junction and hence vary the amount of excess current. This did not occur in our junctions.

In summarizing the preceding results, we can say with confidence that the Ta-Ta$_x$O$_y$-Pb tunnel junctions that we have prepared using a 2-keV argon-ion etching beam have a thin argon implanted normal Ta layer over the superconducting Ta substrate, thus forming a proximity sandwich which produces a knee in the *I-V* characteristics at $eV = \Delta_{Ta} + \Delta_{Pb}$. In addition the junctions have regions where the tantalum is completely normal, giving rise to an excess current below the voltage corresponding to the sum of the energy gaps.

At this point in the development of our technique for electron tunneling junction fabrication, we realized that if we successively reduced the energy of the etching ions, the thickness of the normal layer would also be reduced. At 500 eV, the theory of ion implantation predicts that the argon ions will penetrate tantalum to a depth of approximately 2.5 Å which is equivalent to a Γ_N of 12.5 meV. Figure 5 shows that Γ_N values greater than 10 meV will show no trace of the proximity-induced knee. Experimentally, we fabricated sets of Ta-Ta$_x$O$_y$-Pb tunnel junctions in which we successively reduced the energy of the etching argon ions from 2 keV to 1 keV to 500 eV, and verified that by reducing the energy of the etching ions, we reduced the thickness of the normal layer in the proximity sandwich. Figure 10 shows the *I-V* characteristics for a Ta-Ta$_x$O$_y$-Pb tunnel junction prepared in this way, and a marked reduction in the proximity induced knee can be observed. The data in Fig. 10 yields a value of 0.7 meV for the energy gap of tantalum, which is in complete agreement with the measurements of other workers as can be seen in Table II.

We point out that an absolute comparison of our data on the energy gap of tantalum with the data of other workers is difficult, because in most cases the voltage, which is taken to correspond

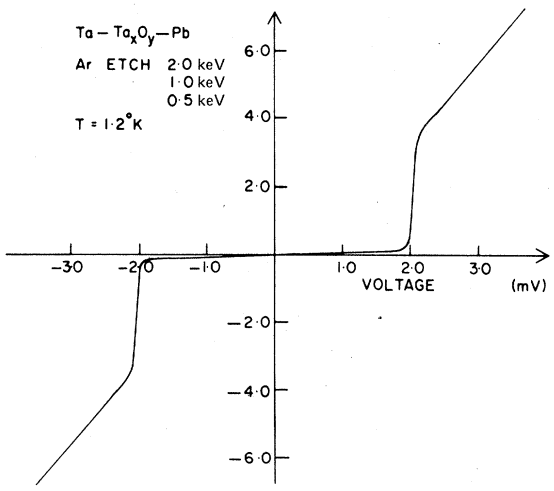

FIG. 10. Experimental current-voltage characteristic for a Ta-Ta$_x$O$_y$-Pb tunnel junction, produced using successive reduction of the voltage of the argon-ion etch from 2 keV to 1 keV to 500 eV, at $T = 1.2$ °K.

to the sum of the energy gaps, is not defined. We use the voltage corresponding to the midpoint of the current rise as the definition of the sum of the energy gaps. We found that for most of our junctions the lead films had an energy gap of 1.35 meV at 1.5 °K. This was deduced by extrapolating the data obtained at higher temperatures where the current peak at the voltage corresponding to the difference of the energy gaps is more pronounced. The energy gap of tantalum below 1.5 °K was taken to be the voltage corresponding to the sum of the energy gaps minus 1.35 meV.

In theory, further improvement of the tunneling *I-V* characteristics is possible by reducing the etching ion energy to an even lower value, until the threshold energy for ion etching is reached when no further cleaning of the sample is possible. Another possibility is to etch with heavier ions. Figure 11 shows that as the mass of the ion is increased, for a given ion energy and target, the depth of penetration of the ions decreases. For example, xenon ions at 1 keV would penetrate tantalum to a depth of only 1.5 Å, and when the ion energy is reduced to 500 eV the penetration depth reduces to 0.75 Å. (It must be remembered that these penetration depths quoted are really average values predicted by theory.) Of course we cannot remove all the implanted ions by reducing the energy and increasing the mass of the etching ions, and for an ultraclean surface the sample would have to be heated to attempt to dislodge the remaining contamination. In order to examine the effect of such thin layers on the tunneling characteristics, one would have to measure dI/dV-V characteristics which are much more sensitive than *I-V* characteristics to proximity effect structure. As can be seen in Fig. 10, a 2.5 Å thick normal layer produced by argon etching at 500 eV produces *I-V* characteristics with almost no trace of the proximity effect visible.

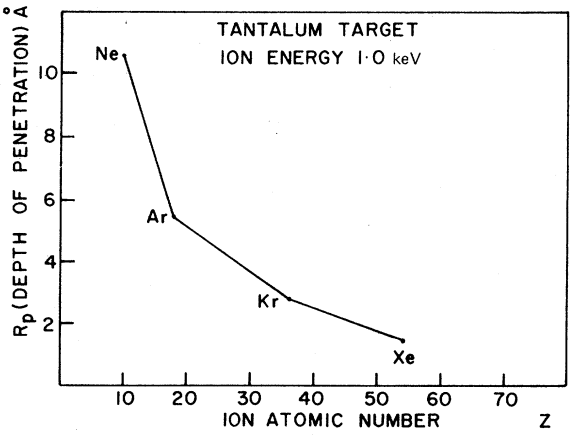

FIG. 11. Plot showing the depth of penetration into a tantalum target of different ions with 1-keV energy.

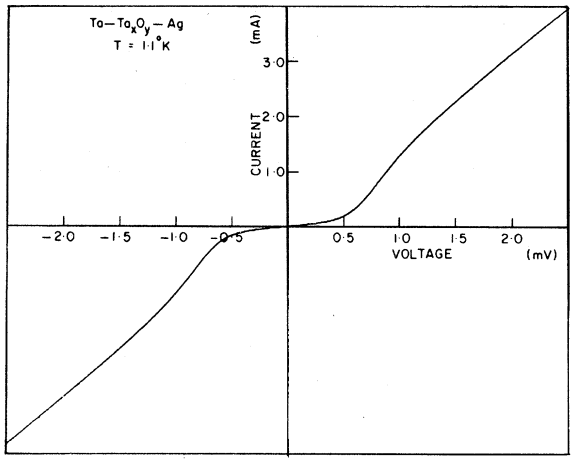

FIG. 12. Current-voltage characteristic of a Ta-Ta_xO_y-Ag tunnel junction at $T = 1.1$ °K.

Our next step was to prepare tantalum tunnel junctions with silver or gold as the normal metal counterelectrode in order to check the quality of the first derivative data obtained from junctions fabricated using our ion etching technique with successive reduction of the etching ion energy. Figure 12 shows the *I-V* characteristic for a Ta-Ta_xO_y-Ag tunnel junction prepared in this manner. From the *I-V* characteristic, we estimate the energy gap of tantalum to be 0.7 meV again in accordance with Shen's measurements.[11,13]

The normalized derivative data $(dI/dV)_S/(dI/dV)_N$ vs V obtained for the tunnel junction of Fig. 12 is shown in Fig. 13. The drop in conductance at 12 and 19 meV is due to the transverse and longitudinal phonons, respectively. The conductance data of Fig. 13 on a Ta-Ta_xO_y-Ag tunnel

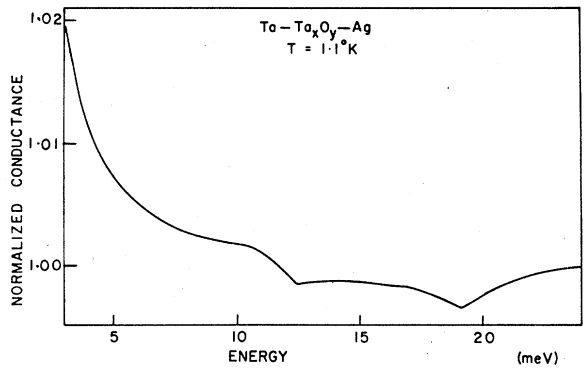

FIG. 13. Normalized conductance, $(dI/dV)_S/(dI/dV)_N$, versus energy $E = eV$ for a Ta-Ta_xO_y-Ag tunnel junction at $T = 1.1$ °K.

junction fabricated on a polycrystalline Ta foil using our method of ion etching is comparable to that of Shen's junction fabricated on an outgassed recrystallized piece of tantalum foil. This shows that the tantalum foils do not have to be heated to a very high temperature to outgas before fabrication of the junction, as was suggested by Shen. The reason for Shen's poor data on the sputtered Ta-Ta_xO_y-Ag junctions may be argon contamination of the surface during the sputtering process. Our experience suggests that if the energy of the bombarding argon ions had been reduced the data would have been comparable to that of his outgassed samples. Further analysis of the conductance data of Fig. 13 to yield $\alpha^2(\omega)F(\omega)$ using McMillan's inversion program was not undertaken because we felt that the analysis would not yield any new information.

B. Niobium

Having successfully fabricated electron-tunnel junctions on tantalum using our new technique, we turned our attention to the problems of junction fabrication on niobium. Shen estimates that the tunneling electron penetration depth for niobium is approximately one-half that of tantalum, since v_F is of the same magnitude and T_c doubles in value. Therefore, at the longitudinal phonon energy (24 meV) the tunneling electron penetration distance for niobium is approximately 30 Å. This suggests that surface cleaning is even more important for niobium than it is for tantalum.

With this in mind we proceeded to fabricate Nb-Nb_xO_y-Pb tunnel junctions by the technique described in Sec. II. The polycrystalline niobium was chemically etched and then an insulating layer was formed by anodic oxidation. The tunneling area was defined by ion etching a hole through this insulating layer using a 2-keV argon-ion beam. Auger spectra were recorded before and after the ion etch. Figure 14 shows the presence of carbon and nickel as impurities on the niobium oxide surface prior to the ion etch. After the ion etch, as shown in Fig. 15, there is no trace of nickel, but instead we see the presence of argon and nitrogen in addition to reduced amounts of carbon and oxygen. The spectra of Figs. 14 and 15 were analyzed using Eq. (1) to determine the atomic concentrations of the various elements present on the surface of the niobium samples before and after the ion etch. The results of this analysis are summarized in Table III. As in the case of tantalum, the argon concentration is difficult to determine by this analysis because a standard spectrum for a known amount of argon is not available. In Table III, we give an upper limit to the concentration of argon present on the surface of the niobium samples.

Figure 16 shows a typical *I-V* characteristic of a tunnel junction fabricated on polycrystalline Nb using a 2-keV argon-ion etch. We designate these junctions as Nb-Nb_{Ar}-Nb_xO_y-Pb in the same manner as in the case of tantalum. From Fig. 16, it can be seen that these tunnel junctions show very little excess current below the voltage corresponding to the sum of the energy gaps. However, just as in the case of Ta-Ta_{Ar}-Ta_xO_y-Pb

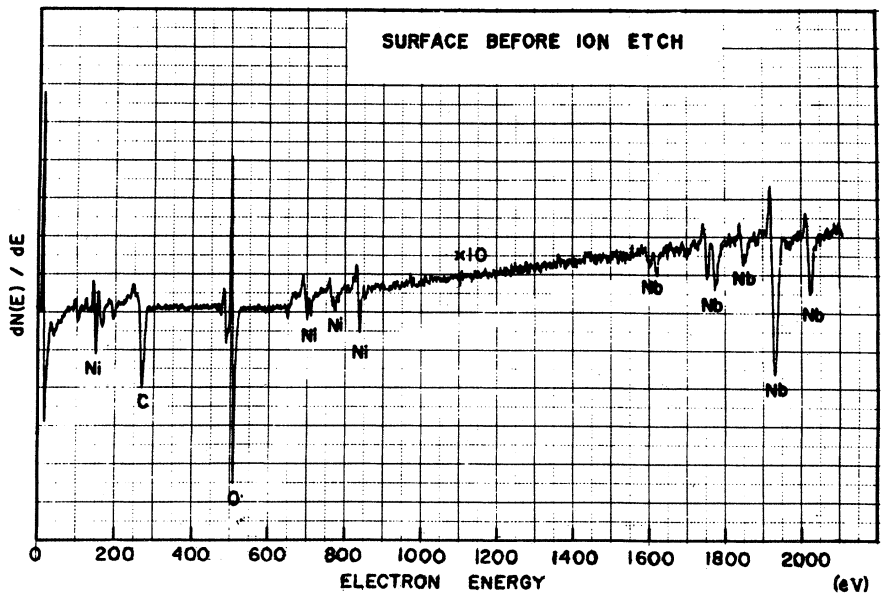

FIG. 14. Auger spectrum of the niobium sample surface at the center of the junction area location before the argon-ion etch.

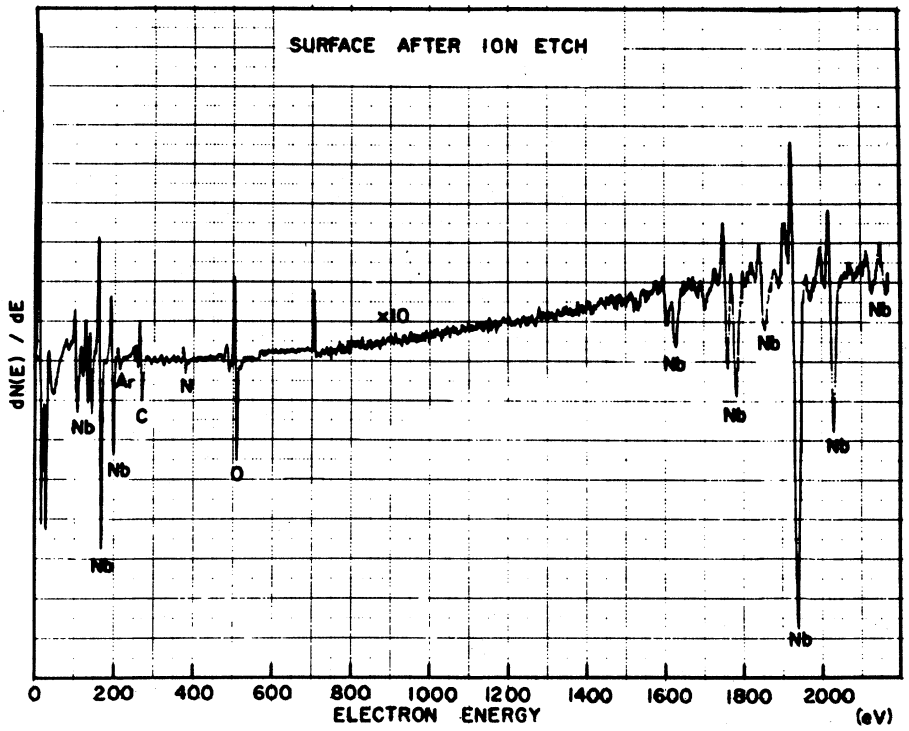

FIG. 15. Auger spectrum of the niobium surface at the center of the junction area after the argon-ion etch.

junctions, Fig. 16 shows that there is pronounced structure just above the voltage corresponding to the sum of the energy gaps. This knee structure is a manifestation of the proximity effect, indicating that we have a thin, contaminated layer on the surface of our niobium. As in the case of Ta, the knee structure shown in Fig. 16 becomes smaller and less pronounced as the temperature is increased and it eventually disappears. The sum of the energy gaps as derived from the *I-V*

TABLE III. Atomic concentrations of the various elements present on the surface of a Nb foil in the center of the junction area before and after the argon-ion etch.

			Initial			
Element	Ar	C	N	O	Ni	Nb
$S_{\alpha,\mathrm{Ag}}$	0.0289	0.1106	0.1824	0.5106	0.2541	0.0137
I_α	0.0	139	0.0	410	9	25.25
$\frac{I_\alpha}{S_{\alpha,\mathrm{Ag}}}$	0.0	1256.78	0.0	802.98	35.42	1843.07
C_α	0.0%	31.9%	0.0%	20.4%	0.9%	46.8%
			Final			
I_α	15	100	35	235	0.0	62
$\frac{I_\alpha}{S_{\alpha,\mathrm{Ag}}}$	519.03	904.16	191.89	460.24	0.0	4525.55
C_α	7.9%	13.7%	2.9%	7.0%	0.0%	68.5%
C_α without Ar	0.0%	14.8%	3.2%	7.6%	0.0%	74.4%

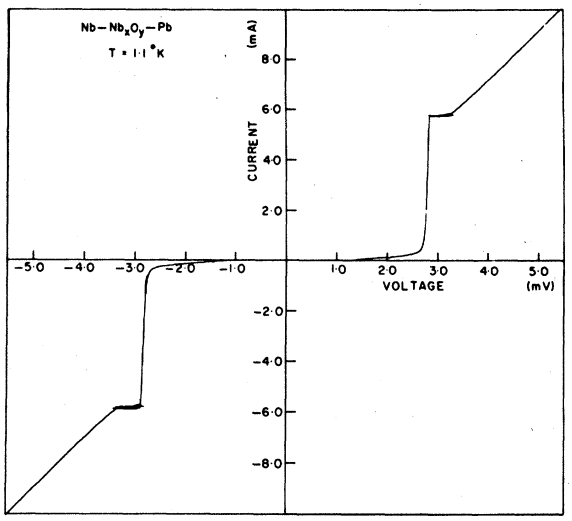

FIG. 16. Current-voltage characteristic of a Nb-Nb_{Ar}-Nb_xO_y-Pb tunnel junction fabricated using a 2-keV argon-ion etch.

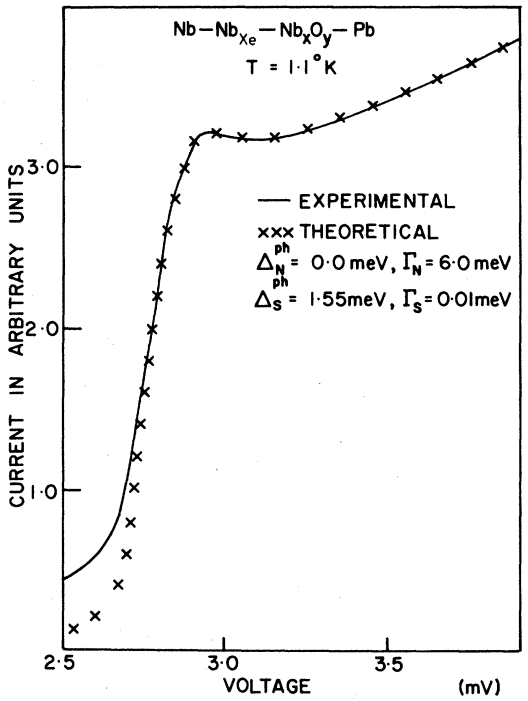

FIG. 17. Portion of the calculated current-voltage characteristic (×××) with $\Delta_S^{ph}=1.55$ meV, $\Delta_N^{ph}=0.0$ meV, $\Gamma_S=0.01$ meV, and $\Gamma_N=6$ meV compared with the experimental curve (solid line) for a Nb-Nb_{Xe}-Nb_xO_y-Pb tunnel junction at 1.1 °K.

characteristic of Fig. 16 is 2.81 meV. This leads to a value of 1.46 meV for the energy gap of niobium at 1.1 °K instead of the much higher value of 1.56 meV observed by Bostock *et al.*,[5] Frommer *et al.*,[36] and Broom.[37]

Instead of fitting the *I-V* characteristics of our Nb-Nb_{Ar}-Nb_xO_y-Pb tunnel junctions using MTM, we thought that it would be more instructive to fabricate some Nb-Nb_{Xe}-Nb_xO_y-Pb tunnel junctions for such a comparison. In this way we might test whether the heavier xenon ion did indeed penetrate less than the lighter argon ion, and thus possibly obtain a different normal layer thickness for testing the applicability of MTM. We prepared these Nb-Nb_{Xe}-Nb_xO_y-Pb tunnel junctions by following all the customary steps except that we substituted xenon gas for argon for the ion etching stage in the fabrication.

Eqs. (6) and (7) obtained from ion implantation theory predict that 2-keV xenon ions should penetrate niobium to a depth of 4 Å. If we assume that the Fermi velocity v_F for niobium is the same as that for tantalum, then we can use Eq. (9) to obtain an estimate for Γ_N. Substituting $\sigma=0.04$, the value found from the Γ_N value that fit the proximity induced structure in tantalum, and $d_N=4$ Å into Eq. (9), we calculate Γ_N to be 8 meV.

Using $\Gamma_N=8$ meV and $\Gamma_S=0.01$ meV as a guide just as in the case of tantalum, we solved numerically the MTM Eq. (16) for $\Delta_S(E)$ and $\Delta_N(E)$ using $\Delta_N^{ph}=0.0$ meV and $\Delta_S^{ph}=1.55$ meV and several values of Γ_N and Γ_S. It should be noted that we tried lower values of Δ_S^{ph} in attempting to fit the proximity induced structure, but we found that we needed a value this high to obtain the correct value for the sum of the energy gaps. Figure 17 shows the comparison between the calculated *I-V* characteristic based on MTM and the experimental *I-V* characteristic obtained for a Nb-Nb_{Xe}-Nb_xO_y-Pb tunnel junction. The agreement of the experimental and theoretical curves is excellent above the voltage corresponding to the sum of the energy gaps, but below this voltage the fit is very poor.

From the Γ_N value needed to fit the experimental data of Fig. 17, we can determine σ for the xenon-doped niobium layer on niobium.

$$\Gamma_N = 790/d_N = 6.0 \text{ meV}. \tag{13}$$

Substituting $d_N=4$ Å into Eq. (13), we calculate σ to be 0.03, which is almost the same as that found for the argon-doped tantalum layer on tantalum i.e., $\sigma=0.04$. While both values of σ are very close together, as has been mentioned earlier, they are lower by a factor of approximately 3 than the value of 0.1 for σ found by Adkins and Kington[23] for Cu-Pb or Ag-Pb films and by Toplicar and Finnemore[26] for Pb-Cd films, where in both cases the films were evaporated and the normal layer was hundreds of angstroms thick.

Whether this lower value of σ that we find is caused by the ion implantation process of producing the normal layer, by the extreme thinness of the normal layer, or by one of our assumptions in fitting to MTM is unknown at the present time.

As a check on the thickness of the normal layer used in our fit to MTM, we tried to verify experimentally the thickness of the contaminated layer on the tantalum surface after the argon etch. Tantalum and argon were chosen for this check because this combination gave an Auger peak for argon which was observable and showed the least interference with other Auger peaks from other elements present in the system. The tantalum sample was bombarded with 2-keV argon ions to produce an argon contaminated layer on the surface of the tantalum. Then, an Auger spectrum was taken, and it showed clearly the presence of argon. The system was flushed and the argon etching gas was replaced with krypton. The tantalum sample was then etched using 500-eV krypton ions. An Auger spectrum was taken every ten sec of ion etch until the Auger spectrum showed no change. Figure 18 shows the resulting plot of the height of the argon peak as a function of etching time.

In an earlier experiment, the etch rate for tantalum oxide using 500-eV krypton ions had been established at 0.12 Å/sec. Using this as the etch rate for tantalum we can convert the etching times of Fig. 18 into thicknesses in angstroms. The point at which the argon signal disappears represents the thickness of the argon contaminated tantalum layer. Hence we estimate the thickness of this layer to be 90 sec $\times$0.12 Å/sec, which equals 10.8 Å. This is in excellent agreement with the value of 10 Å determined from the theory of ion implantation.

Thus, these results show that the knee structure that we observe in these Ta-Ta_{Ar}-Ta_xO_y-Pb and Nb-Nb_{Xe}-Nb_xO_y-Pb tunnel junctions is due to the proximity effect and can be explained quantitatively by MTM, in that MTM can fit the reduction in the voltage corresponding to the sum of the energy gaps and the magnitude and shape of the knee using a value of Γ_N, which is consistent with the known thickness of the ion implanted layer.

By successively reducing the energy of the etching ions, i.e., 2 keV to 1 keV to 500 eV, we reduced the thickness of the normal layer at the surface of the niobium. Figure 19 shows the I-V characteristic of a typical Nb-Nb_{Kr}-Nb_xO_y-Pb tunnel junction fabricated in this way, together with a theoretical I-V characteristic calculated using McMillan's model. For the best fit, the Γ_N value had to be increased to 20 meV. From the theory of ion implantation, we calculated the thickness of the normal layer created by etching the niobium surface with 500-eV krypton ions to be 1.7 Å. Using this value for d_N, we estimated σ for krypton-doped niobium on niobium to be 0.04. Figure 19 shows the usual excess current below the voltage corresponding to the sum of the energy gaps that we have attributed to tunneling from normal regions of niobium.

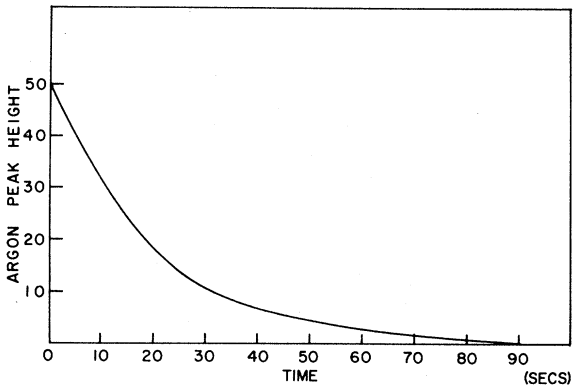

FIG. 18. Plot showing the argon peak height as a function of time while etching with krypton ions through the argon-contaminated tantalum layer.

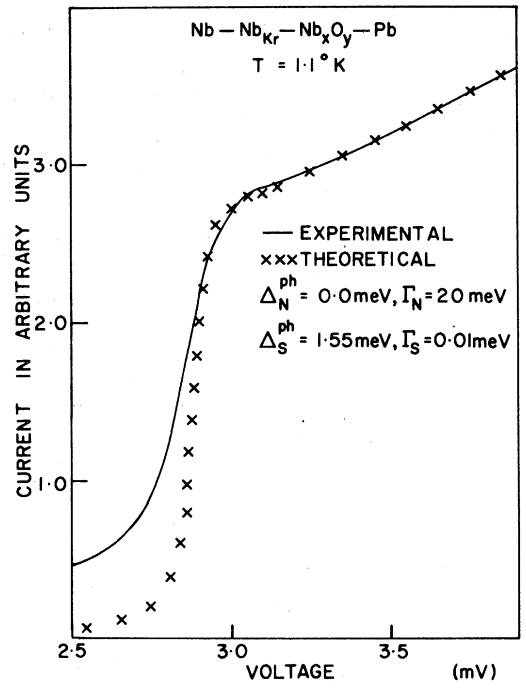

FIG. 19. Portion of the calculated current-voltage characteristic (×××) with Δ_S^{ph} = 1.55 meV, Δ_N^{ph} = 0.0 meV, Γ_S = 0.01 meV, and Γ_N = 20 meV compared with the experimental curve (solid line) for a Nb-Nb_{Kr}-Nb_xO_y-Pb tunnel junction at T = 1.1 °K.

Careful examination of the theoretical and experimental curves of Fig. 19 shows that the structure due to the proximity effect has not been completely eliminated by the final etch at 500 eV. As in the case of tantalum, further improvement in the *I-V* characteristics of the niobium junctions is theoretically feasible either by reducing the energy of the etching ions towards the threshold value for etching or by increasing the mass of the etching ions. However, the nature of the sputter etching process will always leave some ion implantation. Whether heating the sample would help to remove the remaining contamination still needs to be examined, but this would have required further development and was not attempted in connection with this work. The technique that we have developed yields reasonable results for the energy gap of niobium. The *I-V* characteristic in Fig. 19 yielded an energy-gap value of 1.50 meV for niobium at 1.1 °K which, within the limits of experimental error, is in agreement with that of other workers as shown in Table IV. Again, an absolute comparison of our data on the energy gap of niobium with the data of other workers is difficult because, in most cases, the criterion used for determining the voltage corresponding to the sum of the energy gaps is not defined. We use the voltage corresponding to the midpoint of the current rise as the definition of the sum of the energy gaps.

Our directly measured value for the energy gap of niobium at 1.1 °K is in good agreement with those values obtained by Robinson *et al.*[9] and Shen.[11,13] However, it must be remembered that our *I-V* curves still show some evidence of a proximity effect, and therefore our measured value for the energy gap of niobium must be slightly depressed from the true value. This is confirmed by the value of Δ_S^{ph} required to fit the experimental *I-V* curves, and in fact the analysis using MTM requires an energy-gap value of 1.55 meV in the superconducting niobium under the thin normal layer. Thus, our results when the proximity effect is considered are in closer agreement with the results of Bostock *et al.*[5] and Broom,[37] who obtain an energy gap of 1.56 meV for niobium.

TABLE IV. Listing of the observed energy-gap values for niobium.

Reference	$2\Delta_{Nb}$(meV)
Sherill and Edwards (Ref. 38)	3.02
Townsend and Sutton (Ref. 31)	3.05 ± 0.05
Giaever (Ref. 33)	2.90 ± 0.05
Neugebauer and Ekvall (Ref. 35)	2.90 ± 0.05
MacVicar and Rose (Ref. 39)	3.10 ± 0.02
Mullen and Sullivan (Ref. 40)	3.0
Shen (Ref. 13)	2.98
Schwidtal and Finnegan (Ref. 41)	2.79
Frommer *et al.* (Ref. 36)	3.12 ± 0.05
Bostock *et al.* (Ref. 5)	3.12 ± 0.02
Robinson *et al.* (Ref. 9)	2.96
Broom (Ref. 37)	3.12
Wolf and Zasadzinksi (Ref. 42)	3.02 ± 0.04
Keith and Leslie (This work)	3.0 ± 0.05

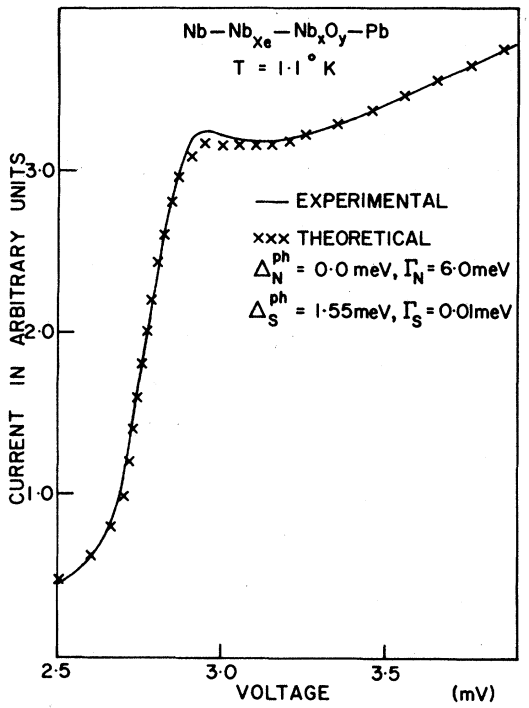

FIG. 20. Portion of the calculated current-voltage characteristic for a Nb-Nb$_{Xe}$-Nb$_x$O$_y$-Pb tunnel junction at $T = 1.1$ °K with 25% of the tunneling current coming from normal areas of the junction.

The excess current below the voltage corresponding to the sum of the energy gaps is due to contaminated regions of niobium which behave as normal material rather than superconducting niobium. Just as in the case of tantalum, we can fit the *I-V* characteristic below $eV = \Delta_{Nb} + \Delta_{Pb}$ by introducing the additional current term given by Eq. (12). By adjusting the value of the parameter K' in Eq. (12) relative to the parameter K in Eq. (8), we can adjust the amount of tunneling current coming from normal regions relative to that coming from superconducting regions of the junction. Figure 20 shows the experimental *I-V* characteristics for the same Nb-Nb$_{Xe}$-Nb$_x$O$_y$-Pb tunnel junction shown in Fig. 17. In Fig. 20, the theoretical curve includes a 25% contribution to the current coming from normal niobium regions, i.e., a normal Nb-Nb$_x$O$_y$-Pb tunnel junction. As can be

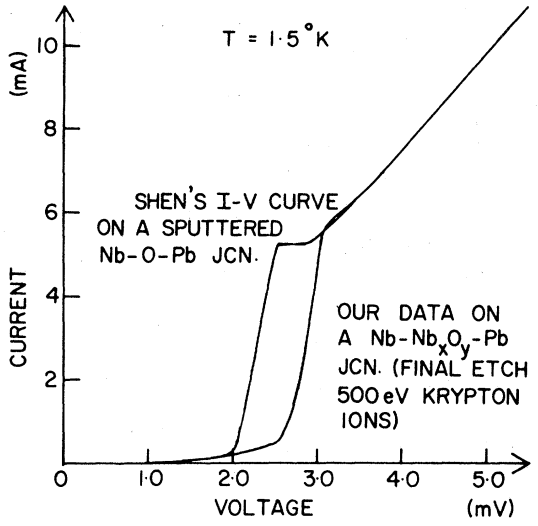

FIG. 21. Comparison of Shen's current-voltage characteristic on a sputtered Nb-O-Pb tunnel junction with a current-voltage characteristic from a Nb-Nb_xO_y-Pb tunnel junction fabricated by our technique of successively reducing the energy of the etching ions.

seen by comparing the theoretical curve of Fig. 20 with that of Fig. 17, we have greatly improved the fit below the voltage corresponding to the sum of the energy gaps at the expense of a small loss of agreement above $eV = \Delta_{Nb} + \Delta_{Pb}$. We feel that the fit between experiment and theory shown in Fig. 20 is really quite good considering that our two-junction model is just a first approximation. In reality, there is going to be a gradual variation of the properties of the niobium around any point where there is contamination. Thus, the energy gap will be zero at the center of the contamination and increase gradually to its full value as we move towards regions where the niobium is clean. The omission of this gradual variation in our model might account for the loss of agreement above $eV = \Delta_{Nb} + \Delta_{Ta}$.

In Fig. 21, we compare the *I-V* characteristic of Shen[11] for a sputtered Nb-Nb_xO_y-Pb tunnel junction with that of a Nb-Nb_xO_y-Pb tunnel junction fabricated by our technique of ion etching and successively reducing the energy of the etching ions. Figure 21 shows that our ion etching technique can produce tunnel junctions on Nb with *I-V* characteristics that are reasonable. We feel that the poor results that Shen obtained using sputter cleaning of his Nb is probably connected both with the sputtering voltage and the gas pressure employed. It should be noted that even when we ion etched using a 2-keV beam of argon atoms in a background pressure of 5×10^{-5} Torr of argon, we never observed the magnitude of depression of the energy gap of Nb demonstrated by Shen's curve in Fig. 21.

The final test for our technique of tunnel-junction fabrication on Nb was to see if it allowed the observation of phonon structure in the tunneling characteristics of a Nb-Nb_xO_y-Au tunnel junction. We prepared tunnel junctions on niobium foils which had been chemically etched and then covered with an insulating layer using anodic oxidation. The tunneling area was defined by ion etching a hole through this insulating layer using 2-keV krypton ions. After clean niobium was reached, the energy of the beam of krypton ions was successively reduced to 1 keV and then to 500 eV. The junction area was thermally oxidized in a pure oxygen atmosphere, and finally gold was evaporated as the counterelectrode to complete the junction. A typical *I-V* characteristic obtained for such a Nb-Nb_xO_y-Au tunnel junction is shown in Fig. 22. The energy gap of niobium estimated from the $I-V$ characteristic of Fig. 22 is 1.50 meV in close agreement with Shen's estimate of 1.49 MeV.

The normalized first derivative curve $(dI/dV)_S/(dI/dV)_N$ vs V of the same junction is shown in Fig. 23. The curve shows a 1% drop in conductance at 18 meV and a much smaller drop of 0.08% at 26 meV. Superimposed on the same graph is data from Shen[11] on a junction fabricated on an outgassed and recrystallized niobium foil. The structure in Shen's data is sharper and stronger than in ours. At 18 meV, for example, the drop-in conductance due to the transverse phonons is of approximately the same magnitude, but in our curve the drop occurs over a wider energy range. As expected, the second drop in conductance at 26 meV, due to the longitudinal phonons, is much

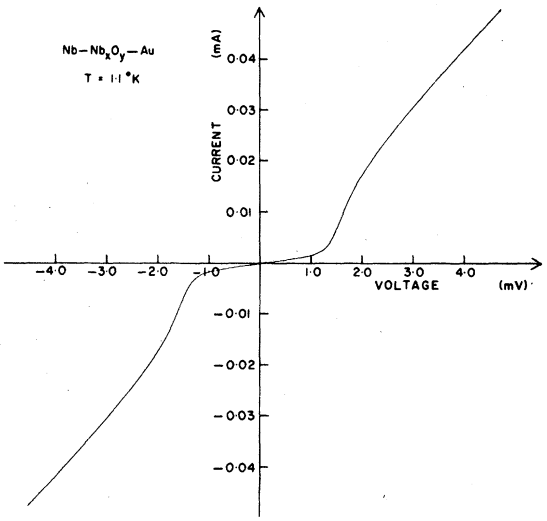

FIG. 22. Current-voltage characteristic of a Nb-Nb_xO_y-Au tunnel junction at $T = 1.1$ °K.

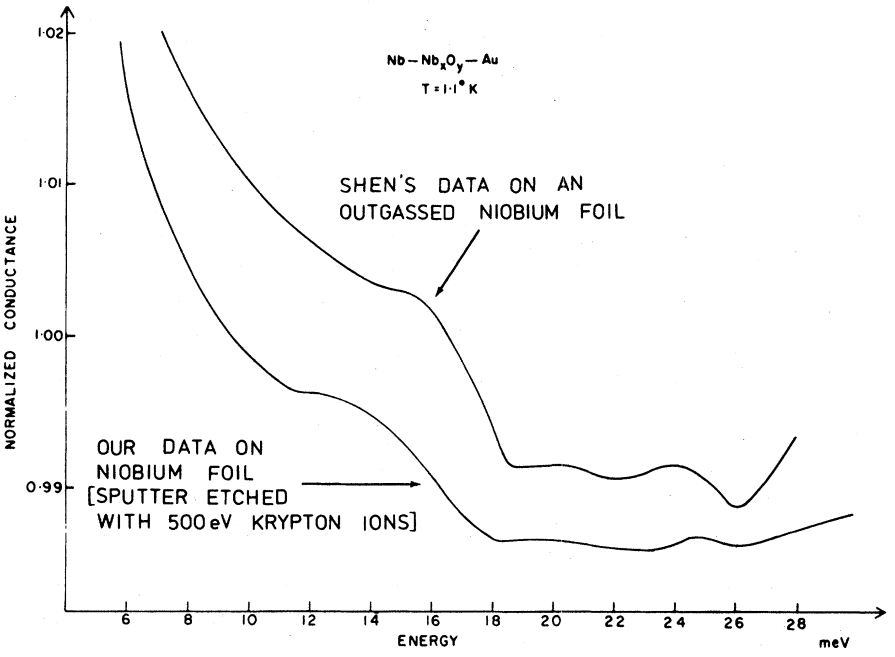

FIG. 23. Normalized conductance curve of a Nb-Nb_xO_y-Au tunnel junction at $T = 1.1$ °K compared with Shen's data of a normalized conductance curve for a Nb-O-Au tunnel junction fabricated on an outgassed recrystallized niobium foil. The two curves have different zeros of conductance to separate them, but the same conductance scale.

smaller than that in Shen's data because of the contaminated surface layer on our niobium samples.

Our data on the normalized conductance of Nb-Nb_xO_y-Au tunnel junctions show that more development of our technique will be required before we will be able to obtain conductance data of sufficient quality that inversion using McMillan's program to obtain details of the phonon structure will be worthwhile. Development of our technique must focus on two areas of concern.

(i) First, the source of the excess current must be clearly identified. We have shown that the problem appears to be due to normal regions on the surface of the superconductor in the junction area. If these normal regions are due to surface contamination, then the use of single-crystal samples with lower amounts of intrinsic impurities should reduce the problem considerably. At present, the grain boundaries in our polycrystalline Nb samples may be allowing impurities to diffuse rapidly to the surface to create centers of contamination on the surface of the Nb.

(ii) Second, the effect of our ion implanted layer on the conductance data must be examined in more detail. Toplicar and Finnemore[26] have shown that phonon spectra derived from proximity sandwiches by a direct application of McMillan's inversion procedure have high-energy tails and an increased value of the Coulomb pseudopotential μ^*. They have shown that a modification to the McMillan inversion procedure can correct approximately for these effects caused by the normal layer in the proximity sandwich. However, their results deal with tunneling into Pb films backed by Cd layers of approximately the same thickness and so are not directly applicable to our situation of tunneling through a very thin normal layer into a much thicker superconducting layer.

Wolf and Zasadzinski[42] have studied electron tunneling through thin Al layers into Nb. They evaporate a layer of Al, 30 to 70 Å thick, onto a freshly outgassed Nb foil at 10^{-9} Torr. The tunnel-junction barrier is obtained by partially oxidizing the Al layer, and they estimate that the resulting Al_2O_3 layer is 30 Å thick. When the Al layer remaining on the Nb is 25 Å thick, the d^2V/dI^2-V data of the In-Al_2O_3-AlNb tunnel junction show sharp strong peaks corresponding to the transverse and longitudinal phonons of Nb and only very weak structure corresponding to the phonons of Al. When the Al layer is 45 Å thick, the corresponding d^2V/dI^2-V data show much stronger Al phonon structure and the peaks associated with the transverse and longitudinal phonons of Nb are weakened and distorted. Wolf and Zasadzinski also express the thickness of the normal layer in terms of the McMillan energy parameter $\hbar v_F/2d_N$, and they find values of 260 and 145 meV for the 25- and 45-Å Al layers, respectively. As can be seen from Eq. (3) with B given its usual value of 1, $\hbar v_F/2d_N$ is equal to Γ_N/σ. In order to compare our results to those of Wolf and Zasadzinski, one would need to know the value of the barrier transmission probability σ for their proximity sandwiches. For example, if σ were 0.1, which is the value found for evaporated layers by Adkins and King-

ton[23] and Toplicar and Finnemore,[26] then Γ_N would be 26 and 14.5 MeV for the 25- and 45-Å Al layers, respectively. Wolf and Zasadzinski suggest that one would expect less scattering or barrier reflection in their AlNb proximity sandwiches and hence a higher value of σ, since the evaporations took place at 10^{-9} Torr rather than 10^{-6} Torr as in the earlier studies.[23,26] However, they have not determined the value of σ for their proximity sandwiches. As we have shown in our MTM fitting shown in Fig. 19, a 1.7 Å thick krypton implanted layer on Nb had a Γ_N of 20 MeV and a σ of 0.03 and was producing a weak proximity effect in the $I-V$ characteristics. How close our Γ_N is to those which apply to the Al layers of Wolf and Zasadzinski could only be determined if we knew their value of σ. Consequently, it is not possible to determine from their results whether the distorted Nb phonon structure that we observe in Fig. 23 is due to too thick an ion implanted layer or is characteristic of contaminated polycrystalline Nb underlying the normal layer. If the latter is the case, then the use of single-crystal Nb samples should improve our phonon spectra considerably. However, we should be able to reduce the thickness of the ion-implanted layer even more by reducing the energy of the ions in the final etch closer to the threshold energy for sputtering. The reason why Wolf and Zasadzinski can obtain such high values of Γ_N/σ for relatively thick layers of Al is due to the fact that v_F of Al is approximately a factor of 10 larger than v_F of Nb. It should be noted that Wolf and Zasadzinski claim that by making the Al layer 30 Å thick, they can completely oxidize the Al layer in the process of forming the tunneling barrier and thus not have any normal layer on the surface of the Nb.

C. La_3Al

In order to test the application of our technique of junction fabrication to more exotic materials, we made a brief attempt to tunnel into La_3Al. A button of La_3Al was made in an argon arc melting furnace. The sample was sliced into discs and the flat surfaces were polished mechanically to a $\frac{1}{4}$-μm finish. The best flat surfaces of the polished discs were then plasma oxidized to produce an insulating layer of approximately 2000 Å. The discs were then mounted on standard-sized foils using silver paint. These mounted samples were then placed in the Auger system and tunnel junctions were fabricated using the procedure described for niobium and tantalum. The tunneling barriers were formed by oxidizing the exposed surface of the La_3Al for approximately 2 min in 50 μm of pure oxygen. Lead was then evaporated as the counterelectrode to complete the junctions.

Figure 24 shows a typical $I-V$ curve for a La_3Al-O-Pb tunnel junction at 1.1 °K. The sum of the energy gaps is 1.6 MeV. This leads to a value of 0.25 meV for the energy gap of La_3Al at 1.1 °K. As can be seen from Fig. 24, the $I-V$ characteristic is not very ideal in that there is much excess current at voltages less than that corresponding to the sum of the energy gaps. The basic problem was that the junctions were unstable and very rapidly became shorts. We tried driving the junctions using an ac current and displaying the $I-V$ characteristics on an oscillo-

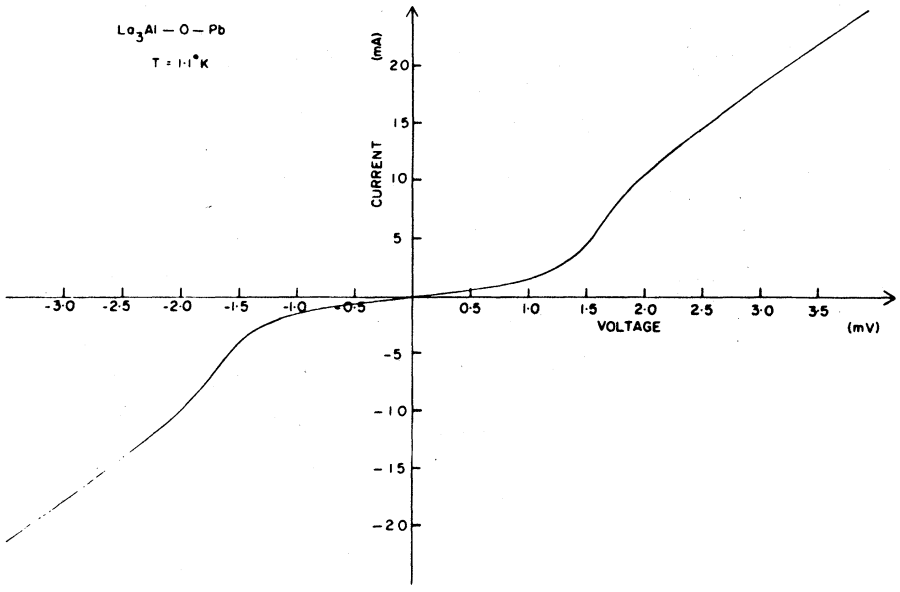

FIG. 24. Current-voltage characteristic of a La_3Al-O-Pb tunnel junction at 1.1 °K.

scope. Occasionally we found a junction that gave a better characteristic initially than the one shown in Fig. 24, but the junction $I-V$ characteristics started to change immediately and head towards a short. Figure 24 represents a junction that lasted long enough to obtain an $I-V$ trace on an $X-Y$ recorder. Because of this problem of junction instability no further measurements were possible.

However, in order to try to understand what was happening to these tunnel junctions, we fabricated more tunnel junctions on La_3Al in the Auger system in the same way, but we used the Auger system to examine them at various stages of their preparation. Two facts were discovered in this way.

(i) The plasma oxidation process appeared to involve mass transfer from the cathode, i.e., oxide ions of the tantalum cathode were migrating to the samples and forming tantalum oxide on the surface of the La_3Al disc. Auger spectroscopy clearly indicated the presence of tantalum oxide on the surface of a La_3Al sample which had been "plasma oxidized." As far as the fabrication technique is concerned, this is not a serious problem. The tantalum oxide simply replaces the oxide of La_3Al as the insulating layer on the surface of the La_3Al.

(ii) The more serious problem was the completed junction. Auger spectroscopy showed that within a very short period of time traces of lanthanum and aluminum could be found on the surface of the lead films which had been evaporated as counter-electrodes. This migration of La and Al was creating shorts in the junctions. The process appeared to be accelerated when an external circuit was connected to the sample and a voltage applied to the junction. A possible explanation is that an electrochemical reaction is taking place because of the difference in the electrochemical potential between the two materials La_3Al and Pb.

While this attempt to tunnel into La_3Al has not been too successful, it should be apparent that the problems encountered are more in the nature of material problems rather than problems with the fabrication technique itself. Indeed, the involvement of Auger spectroscopy in our fabrication technique has demonstrated its power in being able to give information about what was going wrong with the tunnel junctions.

IV. CONCLUSIONS

We have developed a new technique for the fabrication of electron-tunneling junctions on bulk samples of superconductors. The technique involves ion etching a hole through an insulating layer on the surface of the superconducting sample until Auger electron spectroscopy indicates that a clean surface of the superconductor has been attained. Then thermal or plasma oxidation of the clean surface at the bottom of the hole produces the tunneling barrier, and finally a metal evaporation over the hole completes the tunnel junction. We have applied this technique to produce tunnel junctions on bulk samples of Ta, Nb, and La_3Al.

Tunneling into tantalum and niobium has been an excellent test of this fabrication technique in that these transition metals have very short coherence lengths and the tunneling results are very sensitive to contamination of the Ta or Nb surfaces by impurities. We have shown that our fabrication technique produces a thin layer (less than 10 Å) contaminated with implanted etching ions. We have shown that this layer acts as the normal layer in a proximity sandwich, and that it can produce quite large knee structure in the $I-V$ characteristics at voltages just greater than that corresponding to the sum of the energy gaps in a $Ta-Ta_xO_y-Pb$ or $Nb-Nb_xO_y-Pb$ tunnel junction. We have fitted our $I-V$ characteristics with this proximity induced structure to MTM[20] and found quantitative agreement between the theory and the experimental results. In particular, MTM can fit the reduction in the voltage corresponding to the sum of the energy gaps and the magnitude and shape of the kneee structure using a value of the MTM parameter Γ_N which is consistent with the known thickness of the normal layer determined in an independent etching experiment. The barrier transmission probability σ between the normal layer and the underlying superconducting layer turns out to be 0.03 to 0.04 for all our samples, significantly lower than the 0.1 value of σ found by Adkins and Kington[23] for Cu-Pb or Ag-Pb films and Toplicar and Finnemore[26] for Pb-Cd films.

We propose that the excess current observed in the $I-V$ characteristics of our $Ta-Ta_xO_y-Pb$ and $Nb-Nb_xO_y-Pb$ tunnel junctions below the voltage corresponding to the sum of the energy gaps is due to regions of the transition metal within the junction area which are behaving as normal metal. Thus, this excess current is the result of a normal metal–oxide–lead tunnel junction, in parallel with the transition-metal–oxide–lead tunnel junction. Using this two-junction model in conjunction with the $I-V$ calculations based on MTM, we can fit the experimentally observed $I-V$ characteristic quite well over the entire voltage range. Typically, we have to assume that up to 25% of the total junction current is coming from these normal regions. We have not been able to identify the source of these normal regions, but we suspect

that they are caused by impurities diffusing out of the sample along grain boundaries and producing centers of contamination on the ion cleaned surface. It is interesting to note that there is a tendency for the samples with the thickest ion-implanted layer, i.e., those produced by a 2-keV ion etching beam, to show the least amount of this excess current associated with normal regions. This fact would be consistent with our explanation of the origin of this excess current, if the implanted etching ions were tending to block the other impurities in the sample from diffusing to the surface.

We have shown that we can reduce the thickness of the layer implanted with etching ions by successively reducing the energy of the etching ions, i.e., 2 keV to 1 keV to 500 eV, during the ion etching of the surface. This has allowed us to do two things. First, it has substantiated our interpretation that the knee structure in the I-V characteristics of our Ta-Ta_xO_y-Pb and Nb-Nb_xO_y-Pb tunnel junctions above the voltage corresponding to the sum of the energy gaps is the result of a proximity effect between this normal layer and the underlying superconductor by allowing us to demonstrate that as the thickness of the normal layer is reduced the knee structure is reduced in agreement with MTM. Secondly, by reducing the thickness of this normal layer, we are able to get closer to the tunneling characteristics associated with clean surfaces of these transition metals. Indeed, in the case of tantalum, we have made this normal layer so thin that there is a negligible proximity induced knee structure in the I-V characteristics. Consequently, we have been able to obtain from our tunneling measurements the value of 1.40 ± 0.05 meV for $2\Delta_{Ta}$, which is in excellent agreement with the best measurements on clean Ta. In the case of Nb, we have not been able to make this normal layer thin enough, using a final etch of 500-eV krypton ions, to completely eliminate the proximity induced knee structure. Consequently, although the value of $2\Delta_{Nb}$ that we obtain directly from our I-V characteristic is 3.00 ± 0.05 meV, in excellent agreement with the value of 2.96 meV obtained by Robinson *et al.*,[9] the fit to our I-V characteristics using MTM requires the Nb underlying the normal layer to have $2\Delta_{Nb}$ equal to 3.10 meV. This supports the claim of Bostock *et al.*[5] that $2\Delta_{Nb}$ for clean Nb is $3.12 + 0.02$ meV.

Our data on the normalized conductance of Nb-Nb_xO_y-Au and Ta-Ta_xO_y-Ag junctions prepared using our ion etching technique indicate that more development of the technique will be required before we will be able to obtain conductance data of sufficient quality that inversion using McMillan's program to obtain details of the phonon structure will be worthwhile. In order to improve the quality of our conductance data, we must focus on two areas of concern, i.e., the source of the excess current and the exact effect of the ion-implanted layer on the conductance data at the phonon energies. By applying our technique to single-crystal samples with lower amounts of intrinsic impurities, we should be able to explore whether the excess current is associated with surface contamination originating from the bulk. By lowering the energy of the ions used in the final etching process towards the threshold for sputtering, we should be able to reduce the thickness of the ion implanted layer even more and examine what effect this has on the conductance data.

The technique that we have developed lends itself to junction fabrication on more exotic materials, such as alloys, which are hard to evaporate. The work so far indicates that it is possible to fabricate tunnel junctions on materials such as La_3Al, but that the junctions are somewhat unstable. The problems appear to be material related and not fundamental to the technique. The only fundamental problem that might arise with the use of our technique on alloys is the possibility of differential etching, i.e., the possibility that one constituent of the alloy might ion etch at a different rate than another, and thus leave a surface which does not have the correct stoichiometry. This possibility and material related problems, such as have been experienced with La_3Al, are amenable to investigation by Auger-electron spectroscopy, which is an integral part of our junction fabrication technique.

We feel that our junction fabrication technique at its present stage of development is adequate to tackle a number of problems. It should be ideal for tunneling into superconductors with reasonably large coherence lengths. The use of our technique should make it easier to tunnel into surfaces of single crystals with known orientation of various sp-band superconductors to investigate the existence of energy-gap anisotropy.[28,29] It should be possible to use our technique for preparing a clean superconductor-oxide barrier interface, which can then be exposed to a known amount of an adsorbed molecule, as determined by Auger spectroscopy, before evaporating the counterelectrode to complete the tunnel junction. In this way it should be possible to study the strengths of the electron-molecular interactions responsible for the structure in the tunneling characteristics due to inelastic tunneling.[43]

ACKNOWLEDGMENT

This work was based in part on the Ph.D. thesis of V. Keith (University of Waterloo, Ontario, Canada, 1976) (unpublished).

*Present address: Dept. of Physics, Queen's University, Kingston, Ontario, Canada.
[1]I. Giaever, Phys. Rev. Lett. 5, 147 (1960).
[2]L. Solymar, *Superconductive Tunneling and Applications* (Chapman and Hall, London, 1972).
[3]H. J. Levinstein and J. E. Kunzler, Phys. Lett. 20, 581 (1966).
[4]S. von Molnar, W. A. Thompson, and A. S. Edelstein, Appl. Phys. Lett. 11, 163 (1967).
[5]J. Bostock, V. Diadiuk, W. N. Cheung, K. H. Lo, R. M. Rose, and M. L. A. MacVicar, Phys. Rev. Lett. 36, 603 (1976).
[6]J. Bostock, K. H. Lo, W. N. Cheung, V. Diadiuk, and M. L. A. MacVicar, in *Superconductivity in d- and f-Band Metals*, edited by D. H. Douglass (Plenum, New York, 1976), p. 367.
[7]J. Bostock, W. N. Cheung, R. M. Rose, and M. L. A. MacVicar, *Proceedings of the International Conference on Physics of Transition Metals* (August 15-19, 1977, Toronto, Canada), (unpublished).
[8]J. Bostock, W. N. Cheung, R. M. Rose, and M. L. A. MacVicar, *Proceedings of the International Conference on Lattice Dynamics, Paris, 1977* (Flammarion, Paris, 1978).
[9]B. Robinson, T. H. Geballe, and J. M. Rowell, in *Superconductivity in d- and f-Band Metals*, edited by D. H. Douglass (Plenum, New York, 1976), p. 381.
[10]B. Robinson and J. M. Rowell, Proceedings of the International Conference on Physics of Transition Metals, Toronto, Canada, 1977 (unpublished).
[11]L. Y. L. Shen, in *Superconductivity in d- and f-Band Metals*, edited by D. H. Douglass (Plenum, New York, 1972), p. 31.
[12]W. L. McMillan and J. M. Rowell, in *Superconductivity*, edited by R. D. Parks (Marcel Dekker, New York, 1969), Vol. 1, p. 580.
[13]L. Y. L. Shen, Phys. Rev. Lett. 24, 1104 (1970).
[14]G. Carter and J. S. Colligon, *Ion Bombardment of Solids* (American Elsevier, New York, 1968).
[15]J. C. Riviere, Contemp. Phys. 14, 513 (1973).
[16]D. S. Campbell, in *Handbook of Thin Technology*, edited by L. I. Maissel and R. Glang (McGraw-Hill, New York, 1970), Chaps. 5–17.
[17]J. L. Ord, M. A. Hopper, and W. P. Wang, J. Electrochem. Soc. 119, 439 (1972).
[18]J. W. Mayer, L. Eriksson, and J. A. Davies, *Ion Implantation in Semiconductors Silicon and Germanium* (Academic, New York, 1970), Chap. 2, p. 10.
[19]P. W. Palmberg, G. E. Riach, R. E. Weber, and N. C. MacDonald, *Handbook of Auger Electron Spectroscopy* (Physical Electronics Industries, Edina, Minn., 1972).
[20]W. L. McMillan, Phys. Rev. 175, 537 (1968).
[21]P. W. Wyatt, R. C. Barker, and A. Yelon, Phys. Rev. B 6, 4169 (1972).
[22]M. H. Frommer, M. L. A. MacVicar, and R. M. Rose, *Low Temperature Physics-Lt 13*, edited by K. D. Timmerhaus, W. J. O'Sullivan, and E. F. Hammel (Plenum, New York, 1974), Vol. 3, p. 306.
[23]C. J. Adkins and B. W. Kington, Phys. Rev. 177, 777 (1969).
[24]S. M. Freake and C. J. Adkins, Phys. Lett. A 29, 382 (1969).
[25]J. Vrba and S. B. Woods, Phys. Rev. B 3, 224 (1971); 4, 87 (1971).
[26]J. R. Toplicar and D. K. Finnemore, Solid State Commun. 19, 859 (1976); Phys. Rev. B 16, 2072 (1977).
[27]J. M. Rowell and P. H. Schmitt, A. P. S. March Meeting, Atlanta, Georgia (1976) (unpublished).
[28]K. R. Milkove, J. Bostock, and M. L. A. MacVicar, Solid State Commun. 19, 1095 (1976).
[29]M. L. A. MacVicar, J. Bostock, and K. R. Milkove, in *Anisotropy Effects in Superconductors* (Plenum, New York, 1977).
[30]L. R. Testardi, Appl. Phys. Lett. 29, 579 (1976).
[31]P. Townsend and J. Sutton, Phys. Rev. 128, 591 (1962).
[32]I. Dietrich, in *Proceedings of the Eighth International Conference on Low Temperature Physics*, edited by R. O. Davies (Butterworth, London, 1963), p. 173.
[33]I. Giaver in Ref. 32, p. 171.
[34]A. F. G. Wyatt, Phys. Rev. Lett. 13, 160 (1964).
[35]C. A. Neugebauer and R. A. Ekvall, J. Appl. Phys. 35, 547 (1964).
[36]M. H. Frommer, J. Bostock, K. Agyeman, R. M. Rose, and M. L. A. MacVicar, Solid State Commun. 13, 1357 (1973).
[37]R. F. Broom, IBM-Zurich Research Laboratory Report No. RZ 764 (26220) June, 1976 (unpublished).
[38]M. D. Sherill and H. H. Edwards, Phys. Rev. Lett. 6, 460 (1962).
[39]M. L. A. MacVicar and R. M. Rose, J. Appl. Phys. 39, 1721 (1968).
[40]L. O. Mullen and D. B. Sullivan, J. Appl. Phys. 40, 2115 (1969).
[41]K. Schwidtal and R. D. Finnegan, in *Proceedings of the 1972 Applied Superconductivity Conference* (IEEE, New York, 1972), p. 562.
[42]E. L. Wolf and J. Zasadzinski, Phys. Lett. A 62, 165 (1977), and Proceedings of the International Conference on Physics of Transition Metals, Toronto, Canada, 1977 (unpublished).
[43]R. C. Jacklevic and J. Lambe, Phys. Rev. Lett. 17, 1139 (1966).